TN-1760

HANDBOOK FOR DESIGN OF UNDERSEA, PRESSURE-RESISTANT CONCRETE STRUCTURES

by

H. H. Haynes and R. D. Rail

October 1986
(First published September 1976)

DEEP OCEAN TECHNOLOGY

NAVAL CIVIL ENGINEERING LABORATORY
PORT HUENEME, CALIFORNIA 93043

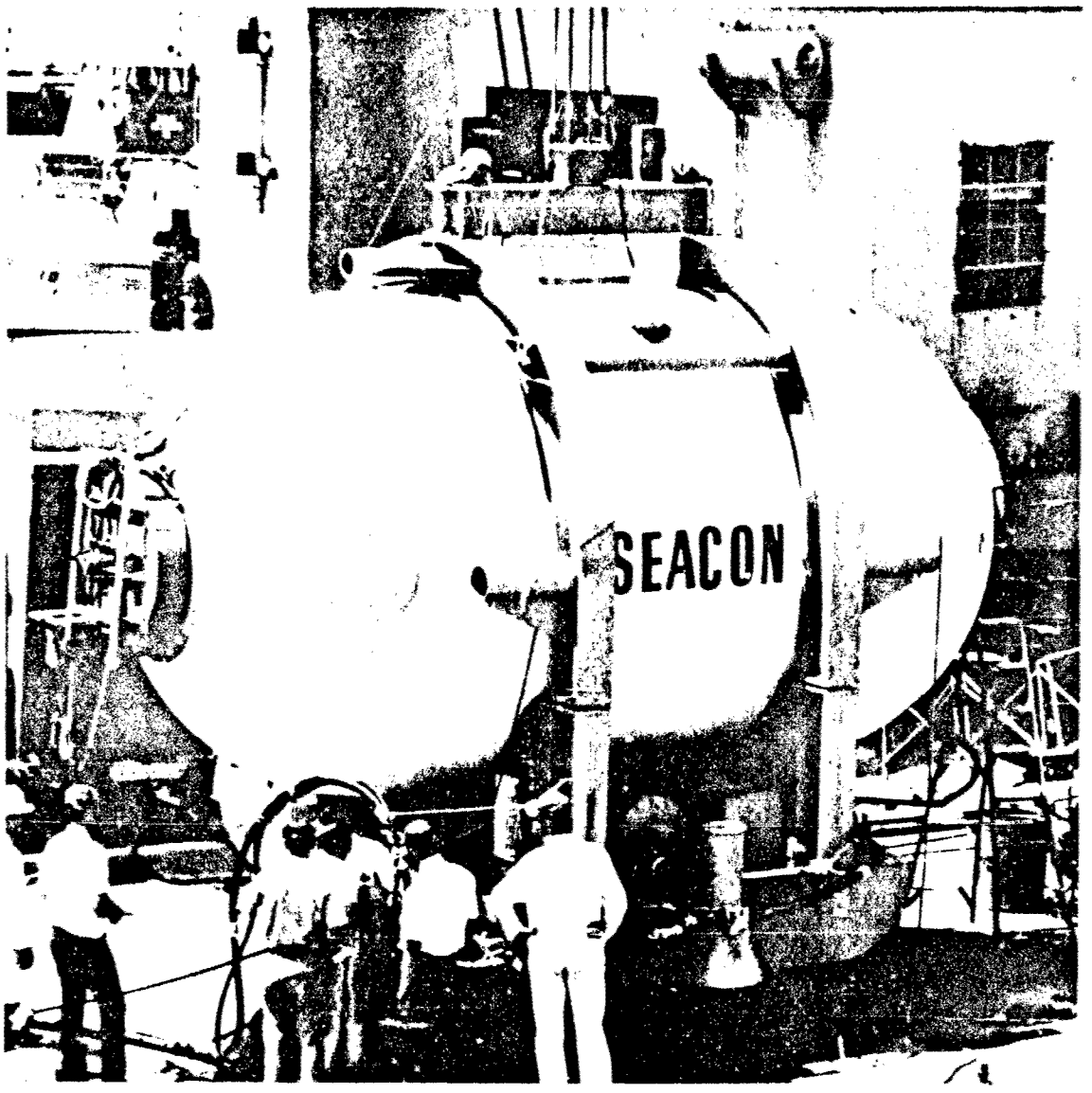

Frontispiece—Concrete cylinder experimental structure, 10-foot OD by 20-foot overall length by 9.5 inch wall thickness, placed on the seafloor at 600-foot water depth for 10.5 months.

Unclassified

SECURITY CLASSIFICATION OF THIS PAGE (When Data Entered)

REPORT DOCUMENTATION PAGE		READ INSTRUCTIONS BEFORE COMPLETING FORM
1 REPORT NUMBER TN-1760	2 GOVT ACCESSION NO DN044053	3 RECIPIENT'S CATALOG NUMBER
4 TITLE (and Subtitle) HANDBOOK FOR DESIGN OF UNDERSEA, PRESSURE-RESISTANT CONCRETE STRUCTURES		5 TYPE OF REPORT & PERIOD COVERED Not final; Sep 1976 – Jan 1985 6 PERFORMING ORG. REPORT NUMBER
7 AUTHOR(s) H. H. Haynes and R. D. Rail		8 CONTRACT OR GRANT NUMBER(s)
9 PERFORMING ORGANIZATION NAME AND ADDRESS NAVAL CIVIL ENGINEERING LABORATORY Port Hueneme, California 93043-5003		10 PROGRAM ELEMENT, PROJECT, TASK AREA & WORK UNIT NUMBERS 63713N; S0397 3.1610-1
11 CONTROLLING OFFICE NAME AND ADDRESS Naval Facilities Engineering Command Alexandria, Virginia 22332		12 REPORT DATE October 1986 13 NUMBER OF PAGES 97
14 MONITORING AGENCY NAME & ADDRESS (if different from Controlling Office) Naval Sea Systems Command Washington, DC 20[illegible]2		15 SECURITY CLASS (of this report) Unclassified 15a DECLASSIFICATION DOWNGRADING SCHEDULE

16 DISTRIBUTION STATEMENT (of this Report)

Approved for public release; distribution unlimited.

17 DISTRIBUTION STATEMENT (of the abstract entered in Block 20, if different from Report)

18 SUPPLEMENTARY NOTES

19 KEY WORDS (Continue on reverse side if necessary and identify by block number)

~~Concrete~~ structures, pressure-resistant structures, concrete spheres, concrete cylinders, submerged concrete structures, undersea structures, long-term loading, unreinforced concrete, compressive strength, cyclic loading, implosion, failure mode, durability, structural design . .

20 ABSTRACT (Continue on reverse side if necessary and identify by block number)

This handbook summarizes the development of concrete pressure-resistant structures for ocean applications and presents the results in the form of design guidelines.

The guidelines are based primarily on test results from laboratory and ocean investigations of model concrete structures conducted at NCEL over the past two decades; the guides are principally for designing cylindrical and spherical plain (unreinforced) concrete structures to resist the externally applied pressures of hydrostatic loads and thus to be safe

continued

DD FORM 1 JAN 73 1473 EDITION OF 1 NOV 65 IS OBSOLETE

Unclassified

SECURITY CLASSIFICATION OF THIS PAGE (When Data Entered)

Unclassified

SECURITY CLASSIFICATION OF THIS PAGE(When Data Entered)

20. Continued

from implosion failure. Thin-walled and thick-walled structures are considered.

For predicting implosion pressure of thin-walled cylinders, buckling expressions by Donnell for moderately long cylinders and by Bresse for long cylinders are simplified by incorporating experimentally determined numerical values for the modulus of elasticity and Poisson's ratio of high strength concrete and then modified by an empirically determined plasticity reduction factor. For thin-walled spheres, a conservative buckling expression was developed.

The design approach for predicting implosion pressures of thick-walled cylinders and spheres is based on material failure in the wall of the structure; the predicted failure stress in the structure is related to the standard concrete compressive strength, f'_c, by empirically derived strength increase factors.

Library Card

Naval Civil Engineering Laboratory
HANDBOOK FOR DESIGN OF UNDERSEA, PRESSURE-RESISTANT CONCRETE STRUCTURES, by H.H. Haynes and R.D. Rail
TN-1760 97 pp illus October 1986 Unclassified

1. Pressure-resistant structures 2. Concrete spheres I. 3.1610-1

This handbook summarizes the development of concrete pressure-resistant structures for ocean applications and presents the results in the form of design guidelines. The guidelines are based primarily on test results from laboratory and ocean investigations of model concrete structures conducted at NCEL over the past two decades; the guides are principally for designing cylindrical and spherical plain (unreinforced) concrete structures to resist the externally applied pressures of hydrostatic loads and thus to be safe from implosion failure. Thin-walled and thick-walled structures are considered. For predicting implosion pressures of thin-walled cylinders, buckling expressions by Donnell for moderately long cylinders and by Bresse for long cylinders are simplified by incorporating experimentally determined numerical values for the modulus of elasticity and Poisson's ratio of high strength concrete and then modified by an empirically determined plasticity reduction factor. For thin-walled spheres, a conservative buckling expression was developed.

The design approach for predicting implosion pressures of thick-walled cylinders and spheres is based on material failure in the wall of the structure; the predicted failure stress in the structure is related to the standard concrete compressive strength, f'_c, by empirically derived strength increase factors.

Unclassified

SECURITY CLASSIFICATION OF THIS PAGE(When Data Entered)

CONVERSION FACTORS—INCH-POUND TO SI (METRIC)

Approximate Conversion Factors (E indicates that the factor given is exact)

To convert from	to	multiply by
Length		
inch	millimeter (mm)	25.4E
foot	meter (m)	0.3048E
yard	meter (m)	0.9144E
mile (statute)	kilometer (km)	1.609
Area		
square inch	square centimeter (cm^2)	6.451
square foot	square meter (m^2)	0.0929
square yard	square meter (m^2)	0.8361
Volume (capacity)		
ounce	cubic centimeter (cm^3)	29.57
gallon	cubic meter (m^3)	0.003785
cubic inch	cubic centimeter (cm^3)	16.4
cubic foot	cubic meter (m^3)	0.02832
cubic yard	cubic meter (m^3)	0.7646
Force		
kilogram-force	newton (N)	9.807
kip-force	newton (N)	4448
pound-force	newton (N)	4.448
Pressure or stress (force per area)		
kilogram-force/square meter	pascal (Pa)	9.807
kip-force/square inch (ksi)	megapascal (MPa)	6.895
newton/square meter (N/m^2)	pascal (Pa)	1.000E
pound-force/square foot	pascal (Pa)	47.88
pound-force/square inch (psi)	kilopascal (kPa)	6.895
Bending moment or torque		
inch-pound-force	newton-meter (Nm)	0.1130
foot-pound-force	newton-meter (Nm)	1.356
meter-kilogram-force	newton-meter (Nm)	9.807
Mass		
ounce-mass (avoirdupois)	gram (g)	28.34
pound-mass (avoirdupois)	kilogram (kg)	0.4536
ton (metric)	megagram (Mg)	1.000E
ton (short, 2000 lbm)	megagram (Mg)	0.9072
Mass per volume		
pound-mass/cubic foot	kilogram/cubic meter (kg/m^3)	16.02
pound-mass/cubic yard	kilogram/cubic meter (kg/m^3)	0.5933
pound-mass/gallon	kilogram/cubic meter (kg/m^3)	119.8
Temperature[6]		
deg Fahrenheit (F)	deg Celsius (C)	$t_C = (t_F - 32)/1.8$
deg Celsius (C)	deg Fahrenheit (F)	$t_F = 1.8t_C + 32$

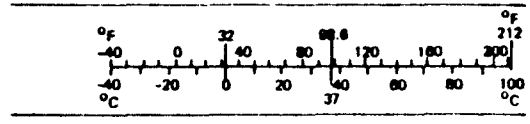

CONTENTS

CHAPTER 1. INTRODUCTION

1.1 OBJECTIVE

This report summarizes the development of concrete pressure-resistant structures for ocean applications and presents the results in the form of design guides. Specifically, the emphasis is on designing concrete spherical and cylindrical structures to withstand implosion failure caused by uniform external hydrostatic pressure loading. Most portions of the design approach are based on experimental data, which have been obtained from laboratory and ocean testing of model concrete structures over the past two decades. Some portions do not have experimental support for the design approach; however, in those cases, extrapolations of the test results have been made in conjunction with theory to give the reader a method for predicting failure that has a quasi-empirical background. This has been done as an alternative to a purely theoretical analysis.

The portions based on experimental studies have been substantially improved in this revised handbook by incorporating additional experimental data and other information obtained in the 10 years since the "Handbook for Design of Undersea, Pressure-Resistant Concrete Structures," was first published in 1976. This is in keeping with the original plan to update the handbook from time-to-time as new information became available. The revisions are included in several ways. For example, information on the uniaxial compressive strength behavior of concrete subjected to long term (to 10.5 years) sustained pressure loading in the ocean, and the behavior of saturated concrete as affected by pore pressure are presented as new sections in Chapter 2. In Chapter 3 an improved method to design cylindrical structures is presented along with simplified design guidelines, for example Figure 3.5. In Chapters 3 and 4, additional data are entered in the curves.

This handbook was prepared as part of the Navy's Deep Ocean Technology Program sponsored by the Naval Sea Systems Command and the Naval Facilities Engineering Command.

1.2 BACKGROUND

In 1966, small model concrete spheres were tested under hydrostatic loading to experimentally determine implosion pressures as compared to theoretically predicted pressures. The results were impressive; for concrete having a uniaxial compressive strength of 10,000 psi, the average circumferential compressive stress in the sphere wall at implosion was 12,500 psi. This 25% higher strength at failure was due, not to any change in the concrete material strength properties, but rather to the geometrical configuration, a sphere, and the loading condition, external hydrostatic pressure. Specifically, the increase in failure strength was the result of the lateral confining stresses caused by the multiaxial compressive loading effects on the wall of the sphere as compared to the uniaxial loading condition of the concrete control specimens (6- x 12-inch cylinders). It was evident from these exploratory tests that concrete could perform well in pressure-resistant undersea structures.

Further studies were conducted on spheres and, later, on cylinders (Ref 1 through 17). The ultimate objectives of the investigations were to determine the maximum depth in the ocean that concrete structures could be safely used and to develop design guides. The results demonstrated the feasibility of near neutrally buoyant concrete structures, having an overall safety factory of three, at depths to 3,000 feet for spheres and 1,500 feet for cylinders. Greater depths are possible if concretes having a compressive strength greater than 10,000 psi are used or if negatively buoyant structures are designed.

During the past 15 years, offshore concrete structures have been used for oil production platforms and storage facilities in the North Sea. This activity has demonstrated the economics and reliability of using concrete in the ocean.

Because of the offshore activity, concrete societies around the world have committed much effort to defining the state-of-the-art and developing recommended standards of practice for concrete ocean structures (Ref 18). The work of these societies will not be repeated herein. As noted this report deals with the special loading case of externally applied hydrostatic pressure. These results have application to concrete floating vessels, offshore platforms, and submerged structures. In addition, hydrostatic pressure loading is a major design load for deep mine shafts and tunnels, and even buried structures subjected to blast overpressures.

Concrete's history is not devoid of examples of submerged pressure-resistant structures. Today many underwater transportation tunnels built of concrete are in operation. A notable example is the BART transbay tube in San Francisco that is 3.5 miles long and located in water 120 feet deep. Interestingly, research related to this report has shown that concrete cylinder structures, such as transportation tubes, can be used to depths 10 times this state-of-the-art depth.

Very large offshore concrete platforms have been built since 1973 for the oil industry in the North Sea. These structures rest on the seafloor with base sections over 300 feet wide and extend above the sea surface with towers having a total height of some 500 feet. The base sections are composed of multiple cells, each cell about 60 feet across and 150 feet high. During construction the cells are employed as pressure-resistant, buoyancy chambers that withstand pressure heads of up to 300 feet. During service the cells are used as oil storage and seawater ballast chambers.

Potential applications in support of military operations are seafloor storage of fuels, long-term environmental data-gathering stations, and possibly target submarines. Feasibility studies have been conducted on fuel storage facilities (Ref 19) and target submarines (Ref 20). The target submarine study showed that a pressure-resistant hull of concrete would cost 60% that of a similar steel hull.

CHAPTER 2. DESIGN CONSIDERATIONS

The design methods presented in this handbook apply to spherical and cylindrical pressure-resistant structures subjected to hydrostatic loading, that is, to external pressure applied normal to the outside surface of the spheres and cylinders (including both the sides and the ends of the cylinders).

This loading places the wall of the structures in a state of multi-axial compression where the inner surface of the wall is in bi-axial compression and all other portions of the wall are in tri-axial compression. For cylinders, the circumferential (hoop) stress is the largest, the longitudinal (axial) stress is less, and the radial (across the wall) stress is the smallest and varies from zero at the internal surface to the same stress level as the applied pressure at the external surface. In a sphere the circumferential stresses are the same in all great circle directions and, again, the smaller radial stress varies across the wall from zero to the ambient applied pressure.

The applied external pressure is assumed to be uniform in all directions and at all locations on the outer surface of the structure. That is, the difference in hydrostatic head at the top and at the bottom of the structure is small compared to the average hydrostatic head and so is neglected.

Although the dead-weight of the structure itself is an important factor in computing the buoyancy of a structure, it is not included in the stress calculations in these guidelines since it is considered to be small compared to the pressure loading. This was the actual situation in the test programs that produced the data on which the design guidelines are based. Thus, these guidelines can be used for design of concrete structures in which the total pressure is a factor of 20 or greater than the pressure difference between the top and bottom of the

structure. These guidelines do not apply directly to cases in which the top-to-bottom pressure difference is a large percentage (10% or more) of the total pressure, for example, the case of a large structure in relatively shallow water. In such situations these guidelines are useful but must be combined with other approaches to account for the nonsymmetry of loading.

The design guidelines in this handbook are presented in equations and charts. These guidelines provide an initial estimate of the size of a structure for a given depth. Advanced design and analysis techniques must be used to complete a final design, but these techniques need to start from given dimensions. This handbook provides design aids to quickly determine the near final dimensions. It is recommended that, once a structure is sized by these aids and meets the design requirements, a detailed analysis (such as a finite element analysis) be conducted. The analysis should assume a realistic out-of-round geometry and take into account any significant loadings due to dead-weight distribution, pressure differentials, live loads, etc.; it should also model the inelastic behavior of concrete materials.

2.1 CONCRETE MATERIALS

2.1.1 Strength

The compressive strength of concrete, f'_c, used in the design equations of this report is the uniaxial compressive strength of 6- x 12-inch control cylinders tested at the time the structure experiences hydrostatic loading. Because the strength of concrete in the as-loaded condition of an undersea structure is needed, the control cylinders should be tested with the concrete in a wet condition. Mature concrete that has been continuously fog cured is considered to be in a wet condition. If the control cylinders have been cured along with the structure and have become air dried from field exposure, the concrete cylinders should be soaked underwater for 3 days prior to testing. However, as will be explained in following sections, concrete that has

been soaked for 3 days is not necessarily "completely saturated." The strength of concrete in a wet condition is about 10 to 20% lower than concrete in a dry condition (Ref 21). Conversely, concrete in a continuously moist condition will gain in strength with aging; at age 1 year, good quality concrete is approximately 20% stronger than at 28 days.

Information is available on the compressive strength of concrete after long periods of time in a hydrostatic environment as reported in References 15 and 17.

Ocean-exposed concrete blocks (18 x 18 x 14 inches) were retrieved on three occasions: 1 block after 1 year in the ocean, 4 blocks after 5.3 years, and 2 blocks after 10.5 years. Six-inch diameter core samples were taken from the ocean exposed blocks and companion on-land field exposed blocks and then tested, along with fog-room cured cast cylinders, for compressive strength, modulus of elasticity, and Poisson's ratio. Drilled cores are, in general, weaker in compressive strength than cast cylinders of the same concrete; for the following strength comparisons the core strengths are adjusted by increasing the measured core strength by 7% as discussed in Reference 15.

The results are summarized in Figure 2.1, which shows the relative strengths of the concrete in the three environments at total ages of 1.3, 5.6, and 10.8 years. The relative strength is the ratio of the compressive strength of the concrete at a given total age compared to the compressive strength at 28 days of fog-cured specimens.

The continuosuly fog-cured specimens increased in strength by 23% at 1.3 years, to 35% above the baseline strength at 5.6 years of age, and were still at 35% at 10.8 years. This pattern of rapid strength gain at early ages and then slower gain and a tendency to level off at later ages is typical of concrete.

The on-land field-exposed concrete, tested in the air-dried condition, showed a similar but smaller gain to 5.6 years, as expected, but indicated a loss of strength during the second 5-year period. This drop, which was not expected, may have been due to differences in the concrete's moisture content, due in turn to the outdoor conditions, especially relative humidity and temperature, which varied considerably

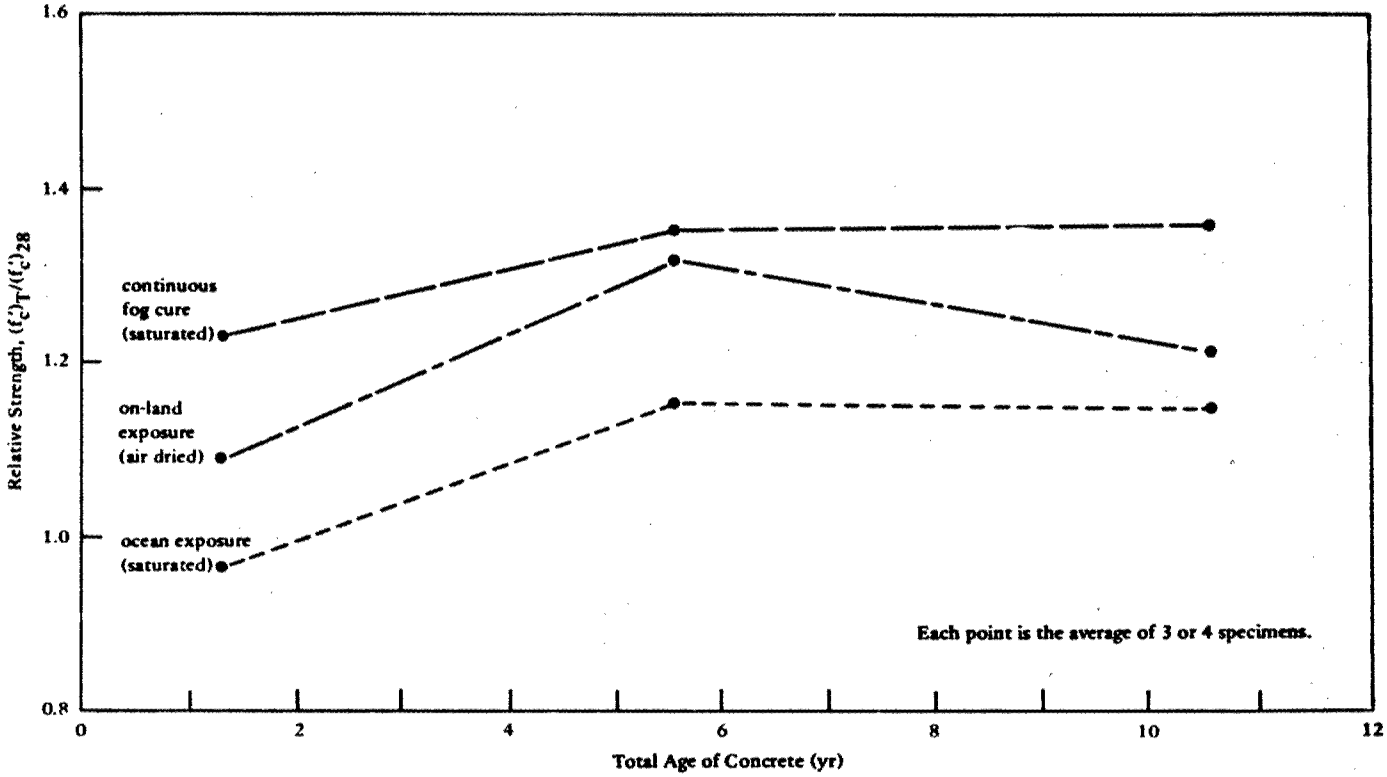

Figure 2.1 Effect of long-term exposure environment on relative compressive strength.*

* Relative strength is the ratio of the compressive strength of concrete at a given total age after exposure in a given environment compared to the compressive strength of the concrete after 28 days of standard cure in a fog room.

on a daily as well as seasonal basis in contrast to the fog room and the in-ocean conditions which were constant throughout the exposure period.

The most interesting findings are, of course, those of the ocean-exposed concrete. This concrete showed a decrease in strength on first being placed in the ocean. This decrease results from the concrete changing from an air-dry condition at the time of deployment (after its initial 28-day cure the concrete was stored outdoors for several months until deployment) to a saturated condition in the ocean. It is well known that the uniaxial compressive strength of wet (saturated) concrete is 10% or more lower than otherwise comparable dry concrete. However, after the initial loss in strength, the concrete continued to cure in the ocean and gain strength. At 1.3 years age its strength was approximately the same as the reference concrete, by 5.6 years total age it was 15% above the baseline strength, and was still at the same strength level at 10.8 years age. Thus, the ocean exposed concrete, after an initial loss, gained strength and then leveled off at the later age, much the same as the reference fog-cured concrete, but at a lower attained strength.

Thus, for predicting strength changes in saturated concrete in the ocean, the data to date indicate that the strength increase of ocean-exposed concrete relative to the 28-day, fog-cured strength is zero at the end of 1 year, 5% at 2 years, and 15% at 5 to 10 years (Ref 17).

2.1.2 Durability

Good quality concrete that is completely submerged in seawater usually does not experience problems of steel reinforcement corrosion. The seawater that eventually surrounds the reinforcing steel becomes oxygen depleted, and the high pH environment supplied by the cement and the products of hydration of the cement, especially $Ca(OH)_2$, acts as an effective method of retarding corrosion.

A potential problem exists in pressure-resistant structures where the interior contains air. Oxygen has access to the walls from inside the structure. Also, the chloride content in the concrete can increase from salts deposited by seawater evaporating on the inside surface thus

promoting corrosion. These problems are accentuated for concrete in the intertidal and splash zones, which are surely the worst environmental conditions to design for durability.

Design criteria include using cement with a suitable tricalcium aluminate (C_3A) content, using concrete with low permeability, and enough concrete cover for the reinforcing steel. The C_3A content should be above 5% but should not exceed 10%, because then the concrete may become vulnerable to deterioration by sulfate attack (Ref 18). Portland cements that meet these specifications are usually Type II or Type V; however, the mill specifications should be used to determine the actual C_3A content. Low permeability is attained for concrete by using: (1) a cement content of 675 lb/yd^3 or greater (do not exceed 840 lb/yd^3 because of shrinkage or heat hydration problems), (2) a water-to-cement ratio of less than 0.45 (and preferably 0.40 or less), and (3) vigorous but not excessive vibration. The use of pozzolans will also help reduce permeability; however pozzolans should be used only after tests have been made to indicate that there is improved sulphate resistance of the concrete and no decrease in corrosion resistance of reinforcing steel (if present). The recommended concrete cover is 2.5 inches on reinforcing steel and 4 inches on prestressing steel. For specific cases, the cover can be reduced by considering aggregate size, bar diameter, cement factor, water-to-cement ratio, workability of fresh concrete, degree of compaction, smoothness of concrete surface, and other factors.

Rock boring mollusks do not usually attack high quality concrete that is made with non-limestone aggregate. As an example, concrete that was located on the ocean side of the Los Angeles Harbor breakwater in California showed only very mild attack by borers after 67 years. In no place had the borers progressed more than 1/4 inch into the surface (Ref 22).

2.2 SATURATED CONCRETE

An understanding of the pore structure of cement paste helps to understand the behavior of saturated concrete.

2.2.1 Pore Structure of Cement Paste

Cement paste composes about 30% of the volume of a good-quality concrete mixture. Because the paste surrounds each aggregate particle and each entrapped or entrained air void, the characteristics of the paste essentially control the permeability of the concrete.

Hardened concrete is a porous material whose void volume is predominately that of the pore space of the cement paste. In general terms, a well-compacted, non-air-entrained concrete (of water-cement ratio 0.40) has a void volume of about 20% at a young age and 14% at a mature age after good curing conditions; the minimum void volume possible is 10%.

Pore size, rather than pore volume, controls the permeability of concrete. In a hardened cement paste, there are essentially two types of pores: capillary pores and gel pores. In a freshly mixed cement paste, the cement particles are rather evenly distributed due to electrostatic repulsion forces. The spaces occupied by the water in the fresh concrete mix are termed the capillary pore spaces; they are interconnected and range in size from 3×10^{-7} inches to 5×10^{-4} inches in diameter (Ref 23). As each cement grain reacts with water, it forms a calcium-silicate-hydrate gel that surrounds the unhydrated portion of the cement grain. With time, fiber-like chains of molecules, called fibrils, develop from the gel coating (Ref 24). The interstices among the fibrils are the gel pores. Gel pores are extremely small, from 4×10^{-8} inches to 3×10^{-7} inches in diameter.

After a cement grain has fully hydrated, the bulk volume of gel is less than the combined volume of the water and cement from which the gel is formed, but is larger (requires 120% more volume) than the original size of the cement grain (Ref 25). The expansion moves into capillary pores. Thus as hydration occurs, the capillary pore volume decreases while the gel volume (and thus the gel pore volume) is created.

Theoretically, if the original water-cement ratio for a paste were 0.38 or less, the entire capillary pore volume would become occupied with gel. The formation of gel within capillary pores increases tremendously the resistance of water molecules moving through the capillary pores. Excellent permeability characteristics arise for concretes made

with water-cement ratios of 0.40 or less because the capillary pores are essentially interrupted or filled by gel.

2.2.2 Seawater Absorption

A major significance of seawater absorption is that large concrete structures can gain in weight by hundreds of tons over long periods of time. Designers may need to consider this factor for certain types of floating, submerged, or relocatable concrete structures.

Two concrete mixtures were tested for seawater absorption (Ref 26). The first mix was a high-quality concrete having a water-cement ratio of 0.39, and a uniaxial compressive strength of 7,380 psi at 28 days. The second mix was a medium-quality concrete of unknown water-cement ratio (about 0.55); the compressive strength was 4,550 psi at 28 days. Specimens of the high quality concrete mix cured for 3.3 years in two different environments: some were exposed continuously in a controlled moist room environment and some to an outdoor environment. The medium-quality concrete was continuously fog cured and the absorption test started at an age of 19 days.

The specimens, which were 6- x 12-inch control cylinders, were subjected to a pressure head of 550 feet and the absorption of seawater was monitored by measuring the quantity of water added to the pressure vessel.

The results of the fog-cured specimens are shown in Figure 2.2. During 8 days time at sustained pressure, the mature high-quality concrete absorbed a negligible amount of seawater. During a similar length of time, the young medium-quality concrete absorbed about 1.1% by weight and then lost about 13% of the absorbed seawater when the pressure was removed and some internal gases expanded.*

Figure 2.3 shows the data for the mature, high-quality concrete that was field-cured for 3.3 years. After 15 days soaking at 0-foot

---

*No specimens were evacuated in any of the test programs because that condition is unnatural for usual concrete applications in the ocean.

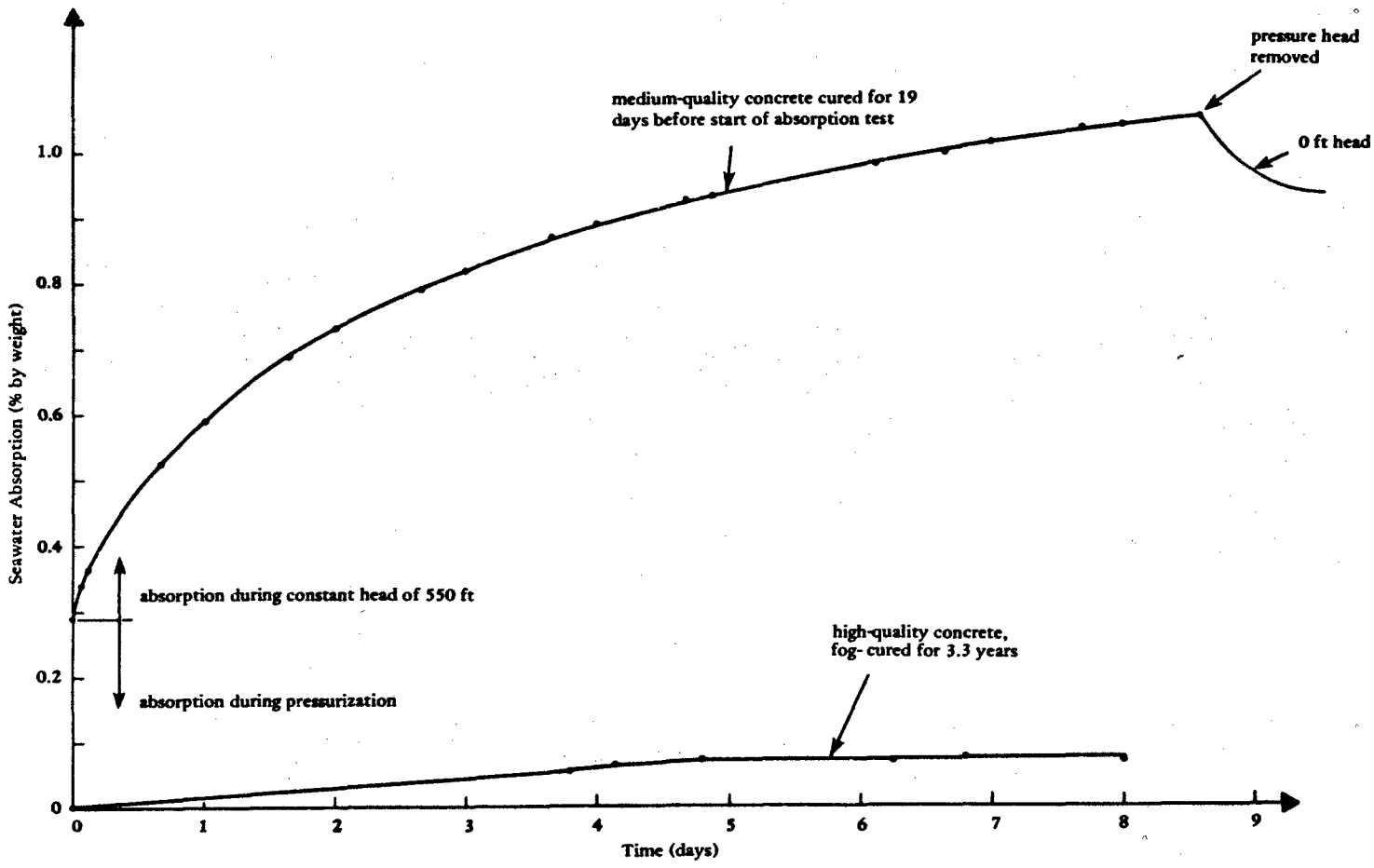

Figure 2.2 Seawater absorption of fog-cured concrete as a function of time under a constant pressure head of 550 feet.

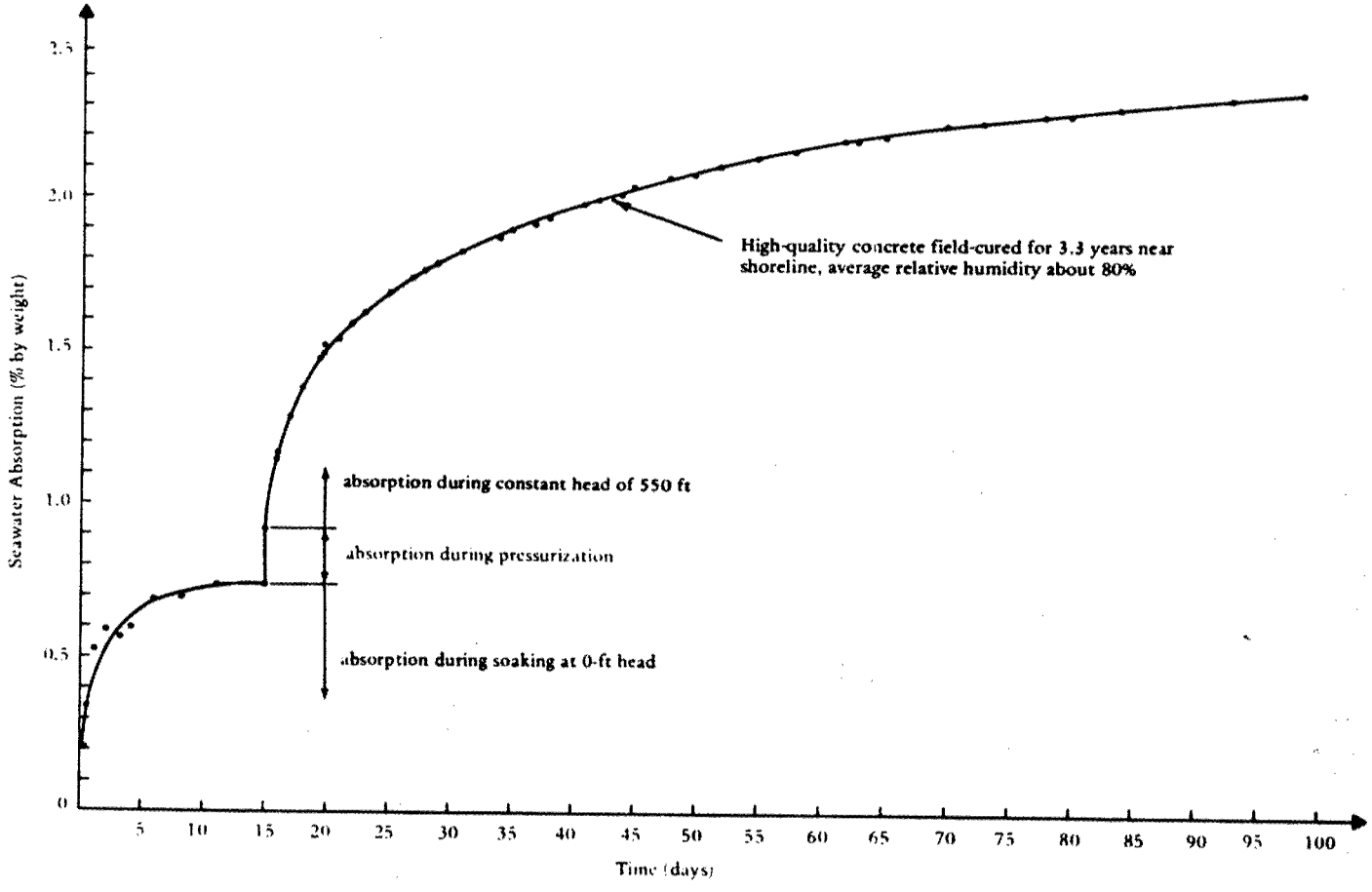

Figure 2.3 Seawater absorption of field-cured concrete as a function of time under a constant pressure head of 550 ft.

head, the concrete appeared to be saturated, but actually was not since more water was absorbed at a 550-feet head. This demonstrates water moving into the gel pores.

The data also illustrate the difficulty of defining "saturated" concrete. At different pressure heads, concrete may become apparently "saturated," yet some gel pores can still be empty.

2.2.3 Compressive Strength of Saturated Concrete

Two types of investigations were conducted on the compressive strength of saturated concrete. During the first investigation mature, high-quality hardened concrete was put into a pressure vessel to saturate the material and then, while at the saturation pressure, a uniaxial compression test (Ref 26) was conducted. During the second investigation freshly mixed concrete, of both high and low strength mixtures, was put into a seawater environment to cure and eventually be tested in uniaxial compression while under the saturation pressure (Ref 27).

The first investigation used a concrete of water-cement ratio of 0.51 and a uniaxial compressive strength of 6,630 psi at 28 days. Specimens were fog cured for 128 days before being placed at pressure heads of 1 foot, 500 feet, and 20,000 feet for about 60 days. The pressure was cycled 4 to 6 times for the 500-foot and 20,000-foot specimens to assist in saturating the concrete.

The results are shown in Figure 2.4. Only the 20,000-foot specimens showed a statistically significant difference in compressive strength from that of the fog-cured specimens. A 10% decrease was recorded. The decrease is attributed to pore pressure build up during the uniaxial test. Under uniaxial load, the change in total volume of the specimen requires that some water be expelled from the specimen. If the rate of loading is faster than internal water can exit the concrete, then a positive pore pressure will develop which can cause a decrease in compressive strength.

The 500-foot specimens showed a 6% increase in strength. The increase could have been due to empty pore space causing the specimen to act as if it were under a small triaxial load from the pressure environment. The 500-foot specimens were not saturated.

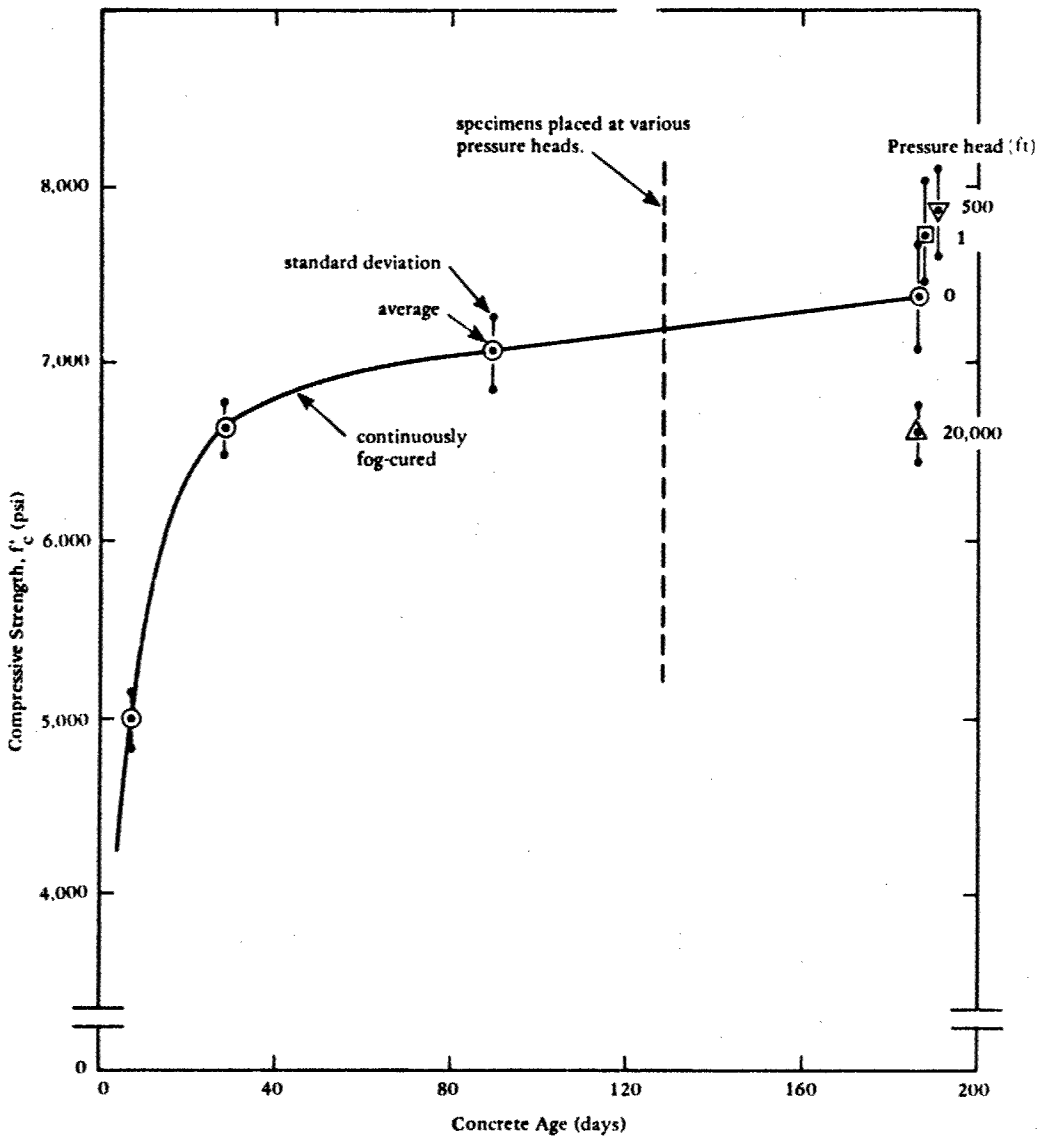

Figure 2.4 Uniaxial compressive strength of concrete tested at various pressure heads.

For the second investigation, specimens of a low-strength concrete mix, which had a water-cement ratio of 0.66 and uniaxial compressive strength of 3,000 psi at 28 days, and a high-strength mix of water-cement ratio of 0.46 and strength of 6,060 psi at 28 days, were placed on the seafloor at a depth of 1,830 feet within 3 hours after mixing before the initial set of the concrete had occurred. After curing in the ocean at 42°F for 11 months, some specimens were returned to the Laboratory, placed again at a pressure head of 1,830 feet for a hold period and then tested under uniaxial compression while at that pressure head. Companion specimens were cured in a fog room at 73°F and others in a tank of continuously circulating fresh seawater at a head of 6 feet at an average of 66°F.

Briefly, the results showed the low-strength concrete increased in uniaxial compressive strength, as compared to the 28-day fog-cured strength, by 28, 28, and 24%, respectively, after 10.8 months of curing in a fog room, 10.2 months in a seawater tank, and 11 months in a deep-ocean environment at 1,830 feet. The differences in strength are not statistically significant, that is, the deep-ocean concrete had a strength essentially equivalent to that of the fog-room and seawater-tank-cured concrete. The high-strength, fog-cured concrete increased in uniaxial compressive strength, as compared to the 28-day fog-cured strength, by 26, 15, and 9% respectively, after 10.8 months of curing in a fog room, 10.2 months in a seawater tank, and 11 months in a deep-ocean environment at 1,830 feet. In this case the differences in strength were statistically significant.

Another group of specimens were retrieved from the ocean after 5 years on the seafloor at a depth of 2,450 feet and tested in the laboratory along with companion specimens that had been continuously cured for the 5 years in a fog room or under a low head (nominally 6 feet) of seawater.

The various specimens were tested in uniaxial compressive strengths under three different conditions: (1) submerged under seawater at the

same pressure (2,450 feet) as the ocean-exposed specimens, (2) under seawater at a low head, and (3) in normal laboratory atmosphere. The results are shown in Figure 2.5 which supplement the findings at concrete ages of 10 to 11 months.

At 5 years age, the low-strength concrete was nearly the same strength that it had been at 10 to 11 months, that is, the low-strength concrete had, essentially, neither gained nor lost strength in the additional 4 years of exposure in the three environments. On the other hand the high-strength concrete continued to gain strength in all three environments. For example, the ocean-exposed concrete averaged more than 30% stronger at 5 years than at 10 to 11 months.

There are several small differences in the strengths of the concretes cured and/or tested in the various environments. For example the low-strength concrete cured and tested (at 5 years age) under high pressure had an average f'_c of 4,100 psi, which is indicative of a reliable, good quality structural concrete, but is about 10% weaker than the companion concrete cured in the near ideal fog room conditions.

However, the main findings of this test series are that, at a given water/cement ratio and a given age (after the first several weeks), the specimens all had similar strengths whether cured or tested submerged at high pressure, submerged at low pressure, or in the air. The differences in performance are primarily due to the well established principles that higher strength is primarily a function of lower water/cement ratio, and the degree of hydration of cement which is a function of age and normally continues (if curing water is available) at a decreasing rate for a number of months up to more than a year, after which the concrete continues to maintain its achieved strength.

2.2.4 Pressure Cycling Effect

Several tests were conducted where concrete was subjected to pressure cycling and then tested under uniaxial compression. This type of test was of interest because a rapid decrease in ambient pressure results in a rapid change in pore pressure of the concrete, a condition which might harm the concrete.

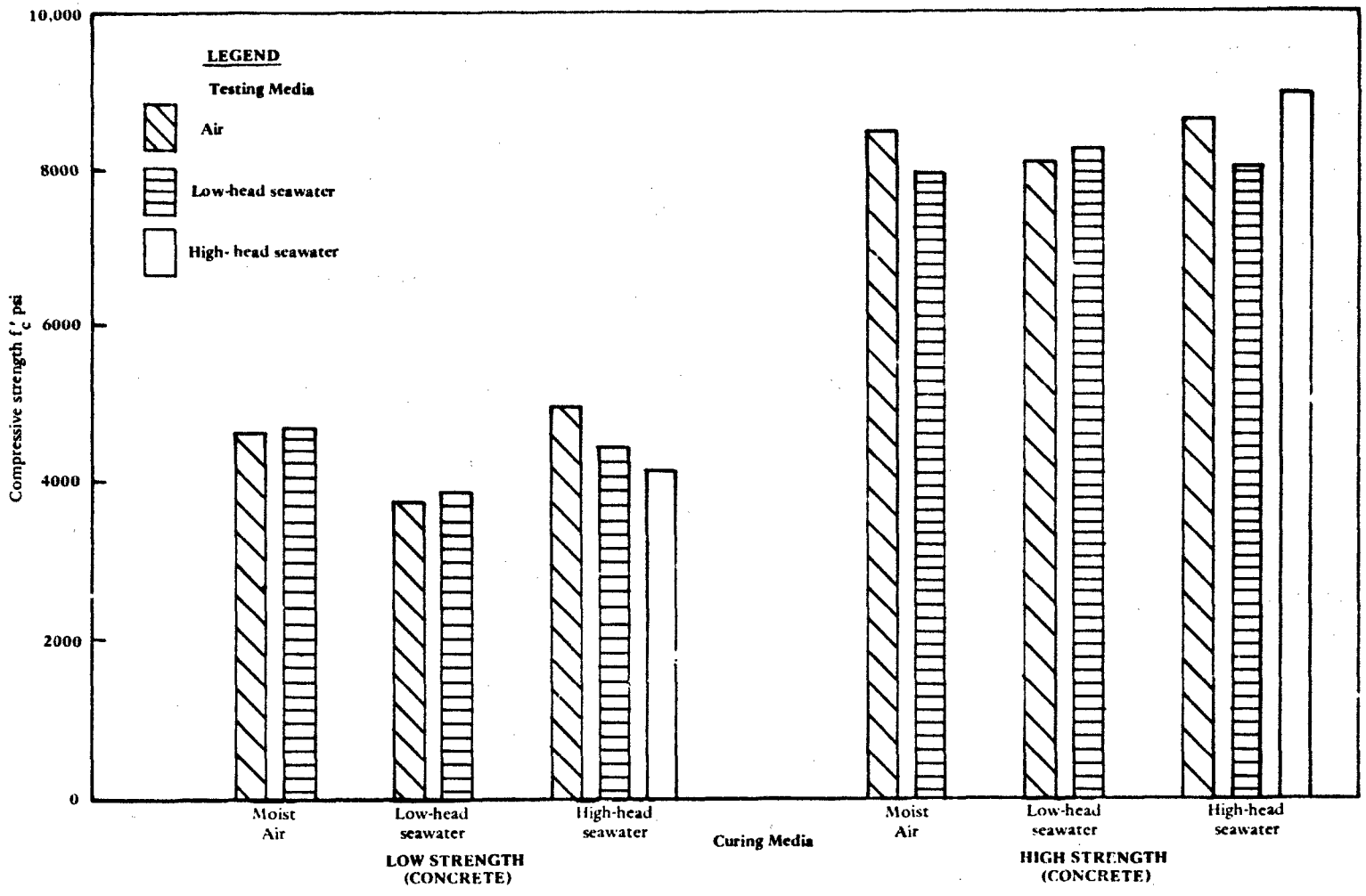

Figure 2.5 Strength of concrete cured and tested in air and seawater at low and high pressure heads.

One test series was part of the program involving freshly mixed concrete placed in the ocean at 1,830 feet. All the specimens, both low-and high-strength mixes, which cured in the ocean for 11 months (and were, therefore, saturated with seawater), underwent three pressure cycles: raised from the seafloor to the surface, placed in a pressure vessel and held at 1,830 feet of head, then removed from the pressure vessel, placed in a compression tester, and then placed back at 1,830 feet of head for the uniaxial test. Each of the pressure cycles was at a rate of 1 foot of head per second (0.4 psi/sec). The strength of these specimens was compared to that of companion specimens that cured in a seawater tank at 6 feet of head. No statistically significant strength differences were observed, so the pressure cycles did not harm the concrete.

Additional ocean-cured specimens of both low- and high-strength mixes were pressure cycled an additional three times at a rate of 10 feet of head per second (4.4 psi/sec). This rate was faster than any concrete structure or object will be raised from the ocean. A practical rate is 1 fps or less. The compressive strength of these specimens was compared to that of the ocean-cured specimens that were exposed to only three cycles of 1 foot of head per second. The strengths were essentially identical, so the faster pressure cycling rate did not harm the specimens.

Another observation that demonstrated that pressure cycling does not harm concrete is the retrieval of two uncoated-concrete spheres from the ocean. One sphere was at 2,790 feet for 5.3 years (Ref 15) and the other sphere at 3,190 feet for 10.5 years (Figure 2.6) (Ref 17). In both cases, after retrieval and a number of hours at atmospheric pressure, the spheres were tested in a pressure vessel to failure by implosion under short-term hydrostatic loading, and behaved similar to spheres that had not been placed in the ocean.

The most significant test of pressure cycling was conducted on six 3- x 6-inch solid, microconcrete cylinders that were exposed to a freshwater pressure head of 45,000 feet for 6 days (Ref 28). The pressure in the pressure vessel was released within 1 second for a depressurization rate of over 45,000 feet of head per second. This condition was an

extreme test. Upon removal from the pressure vessel, the specimens showed cracking as if large areas of the surface were about to spall. Uniaxial compression tests showed that the specimens had an average strength of 5,900 psi. These strength data were compared to that of six companion specimens that had remained in an air-dried (field-cured) condition; these specimens had a strength of 8,040 psi. The decrease in strength was 27%. The strength reduction included the effect of dry concrete becoming wet, which is 10% or more. Hence, only 17% of the reduction would be attributed to the effect of sudden release of pore pressure. Thus, the damage is considered to be small for the extreme nature of the test.

The reason pressure cycling at reasonable rates does not affect concrete is that little water actually moves in or out of saturated concrete as the pressure environment increases or decreases. The bulk modulus of the concrete is a little larger in value than the bulk modulus of seawater; hence, as the pressure increases, the decrease in volume of a concrete specimen is a little less than that of seawater. So a small quantity of seawater will enter the specimen. Upon pressure decrease, the small quality of seawater must exit the specimen. This quantity is about 10 to 20% of the quantity that must exit saturated concrete under uniaxial loading. Hence, pressure cycling does not appear harmful to saturated concrete.

2.3 HYDROSTATIC LOADING CONDITIONS

2.3.1 Long-Term Loading

Experimental investigations on the long-term loading behavior of pressure-resistant concrete structures were conducted primarily on spheres, but a few tests were conducted on cylinders. Three spheres of 16 inches (Ref 1) and seven of 66 inches OD (Ref 10), both sizes having t/D_o ratios of 0.063 (Figure 2.7), were tested in pressure vessels to obtain data on their response to continuously sustained loading during the early period (first 20 days) of long-term loading. Eighteen spheres of 66 inches OD, also having a t/D_o ratio of 0.063, were placed in the

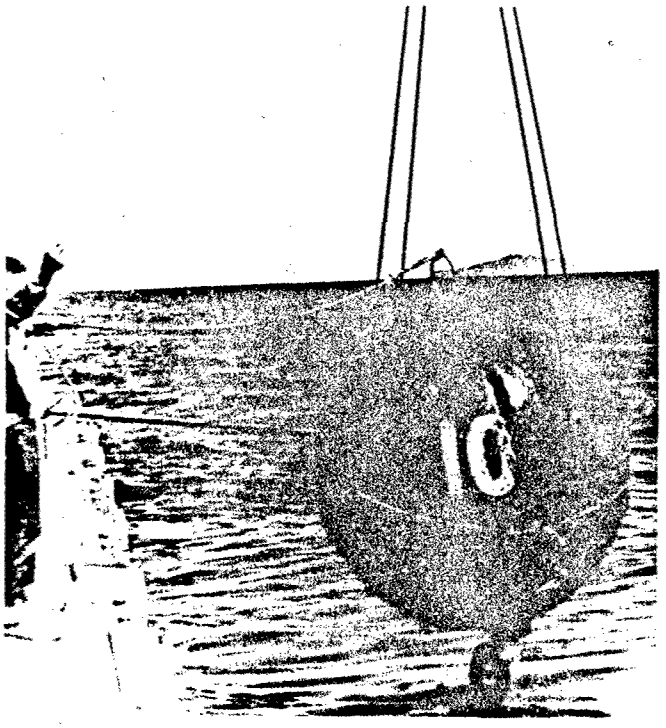

Figure 2.6 Sphere retrieved from 3,190 feet after 10.5 years.

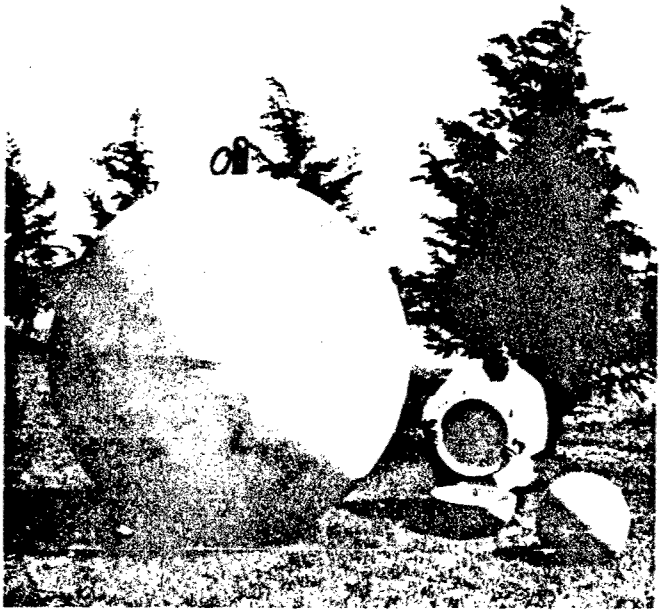

Figure 2.7 Concrete spherical structures, 16-inch and 66-inch OD, used for hydrostatic loading tests conducted in laboratory pressure vessels and in the ocean.

ocean to obtain data for periods up to 13 years and longer (Ref 13, 15, and 17). The spheres were placed in the ocean in 1971; since that time three of the spheres imploded in-situ at or soon after deployment, two spheres flooded without imploding (one soon after deployment with no visible defect, the other due to a small local failure after 8 years in the ocean), five spheres were retrieved from the ocean for laboratory testing, one has never been inspected, and seven are still exposed to long-term loading. The long-term loading data are shown in Figure 2.8.

Three cylindrical specimens, 54 inches OD, with a t/D_o of 0.037 and L/D_o of 2.35, were tested in a pressure vessel (Ref 16 and 29). The data from these tests are also shown in Figure 2.8. A large cylindrical structure (see Frontispiece) of 10 feet OD by 20 feet overall length (10-foot cylinder section plus two hemispherical end caps) was also subjected to long-term loading for 10.5 months in the ocean, but the depth was only 600 feet for a relative load level of about 13% of its short-term strength. The datum from this test is not shown because of the low relative load level (Ref 14).

An average data curve from Stockl (Ref 29), representing hundreds of uniaxial load tests, is shown in Figure 2.8 for comparison. The results compare favorably. This finding shows that dry and saturated concrete under multiaxial stresses behaves in a manner similar to concrete used for on-land structures. There was no unusual behavior observed for concrete used in the deep ocean as compared to the known behavior of concrete under long-term loading.

2.3.2 Cyclic Loading Effect

Previous work on cyclic loading of confined concrete was quite limited. An investigation, therefcre, was conducted on the low-cycle fatigue behavior of fiber reinforced concrete spheres under hydrostatic loading (Ref 30). The spheres were 16 inches OD, with a t/D_o ratio of 0.188.

The concrete mix proportions were a water-cement ratio of 0.43, cement-sand-aggregate proportions of 1:2.55:0.64, and a cement content of 846 lb/yd^3. Type II Portland cement was used along with aggregate,

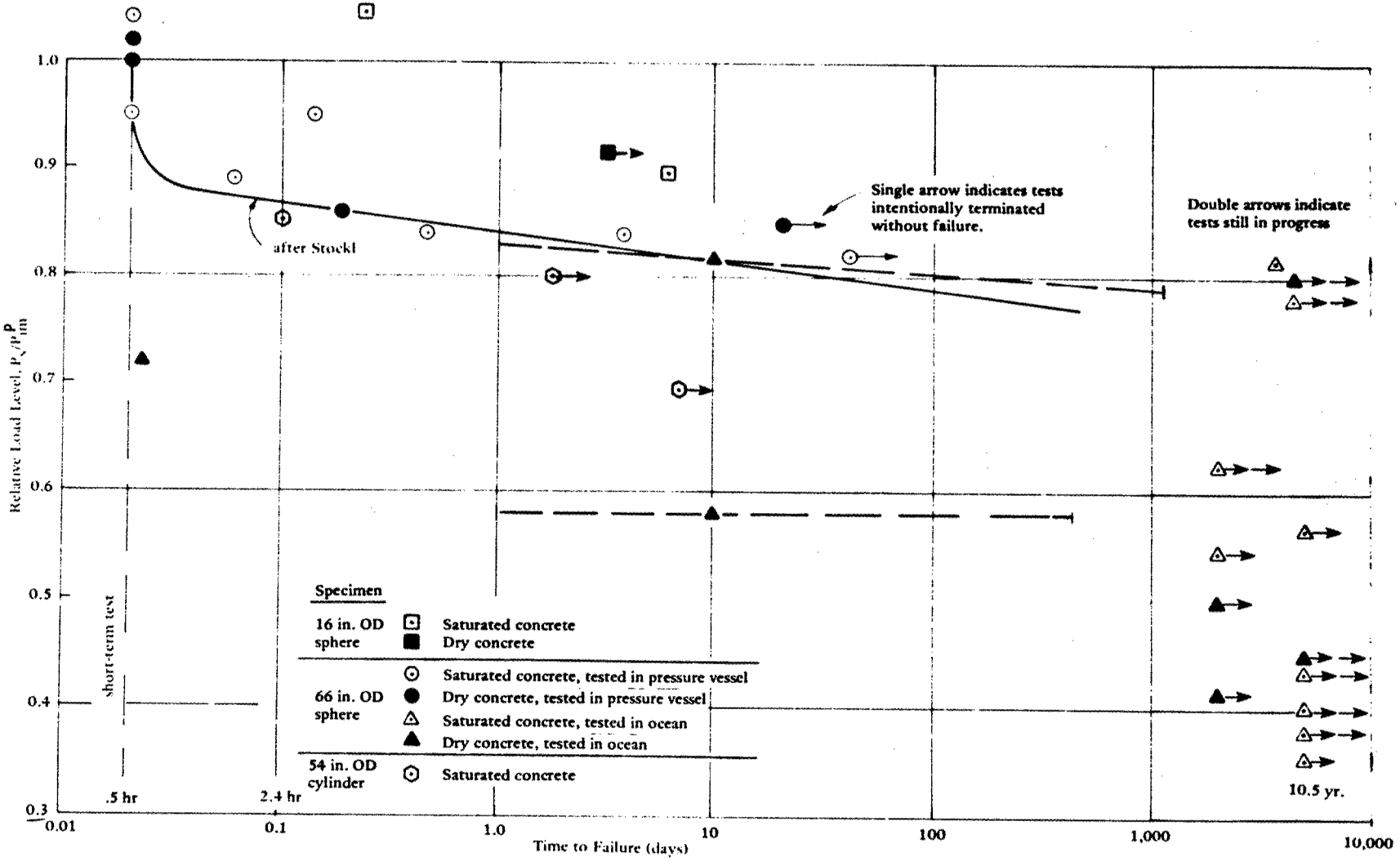

Figure 2.8 Time to failure of concrete spheres and cylinders under long-term hydrostatic loading.

maximum size of 3/8 inch, and a water reducing admixture. Straight steel fibers, 1.5 inches in length and 0.017 inch in diameter, were randomly distributed at a percentage of 1.5% by volume.

The state of stress in the sphere wall varied from biaxial on the inside surface to triaxial elsewhere. The hoop stresses were equal at $\sigma_1 = \sigma_2$ and the radial stress, σ_3, was an average of 0.3 σ_1. The cyclic hydrostatic load cycled all the stresses. This was in contrast to previous work (Ref 31), using plain concrete solid-cylinders, in which the axial stress, σ_1, was cycled from 20% to 80 or 90% of the triaxial ultimate strength while the radial stresses, σ_2 and σ_3, were equal and held constant at stress levels of 9 or 13% of the triaxial ultimate strength.

The test results are shown in Figure 2.9. The spheres showed considerably poorer fatigue behavior compared to the solid cylinders under confinement. This difference in behavior can be explained by the differing stress conditions in the two types of specimens. For the spheres, all wall stresses were cycled, whereas for the cylinders, only the axial stress was cycled. Also, for the spheres, σ_3 was not uniform across the wall but varied from zero at the inner surface to some maximum value at the outer surface.

The sphere results converge rapidly to the uniaxial results (Ref 31 and 32) in Figure 2.9. The uniaxial results should be the lower bound limit of confined concrete fatigue behavior; however, this was not confirmed by the tests.

2.3.3 Rapid Loading

An exploratory test program was conducted on rapidly applying hydrostatic load to concrete spheres (Ref 28). The spheres were 16 inches OD, with a t/D_o ratio of 0.188, and fabricated of plain concrete. The exterior and interior surfaces of the spheres were waterproofed. Previous work on rapid loading effects was conducted only on unconfined concrete solid-cylinder specimens. Testing of spheres under hydrostatic loading provided an opportunity to observe rapid loading effects on confined (unsaturated) concrete.

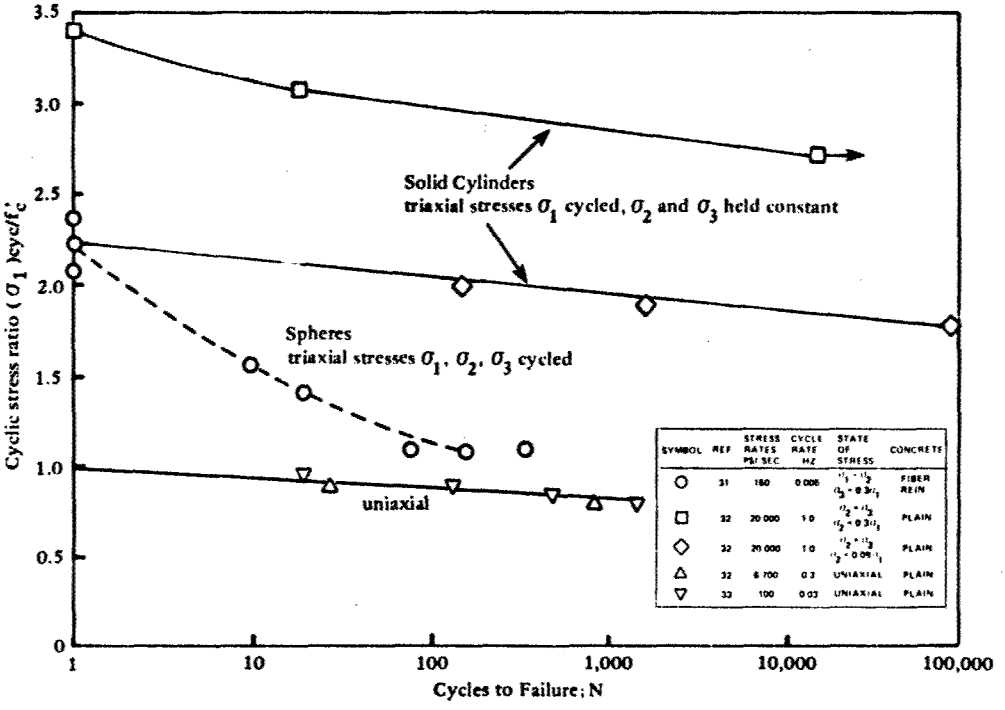

Figure 2.9 Low cycle fatigue behavior of confined and unconfined concrete.

The concrete mix proportions were a water-cement ratio of 0.43, cement-sand-aggregate proportions of 1:2.55:0.64, and a cement content of 846 lb/yd^3. Type III Portland cement, modified to plastic cement by the manufacturer, was used along with an aggregate, maximum size of 3/8 inch, and a water reducing admixture.

The test procedure used for creating a rapid hydrostatic load was to apply an equal pressure of 10,000 psi to the interior and exterior of a sphere, and then quickly release the interior pressure, thereby creating a rapidly applied external hydrostatic load. This procedure, modified by decreasing the interior pressure slowly, was used on two spheres and the implosion results compared well with the previous results on spheres subjected to only external hydrostatic loading (Ref 32, 4, and 30). The average implosion pressure for the two statically loaded spheres was 4,420 psi.

The rapid test procedure was used successfully on two spheres. The external load was applied in about 0.007 second and both spheres resisted the maximum available pressure load of 9,600 psi. One sphere held the pressure for about 0.003 second and the other about 0.025 second; hence, the failures were not instantaneous, but rather creep failures.

The strength results are shown in Figure 2.10 as a function of stress rate and in Figure 2.11 as a function of strain rate. The sphere closest to an instantaneous failure showed a strength increase of 2.3 times that of statically loaded spheres. Past work on rapid loading of unconfined concrete showed strength increases on the order of 1.4 times that of the statically loaded specimens (Ref 33, 34, 35, and 36). The improved strength of the spheres demonstrated that confined concrete resisted rapid loads in a manner superior to that of unconfined concrete.

2.4 REINFORCEMENT

Three studies have considered the effects of steel reinforcement on the implosion behavior of spherical structures. Each study investigated a different reinforcement scheme. Cylindrical structures with steel

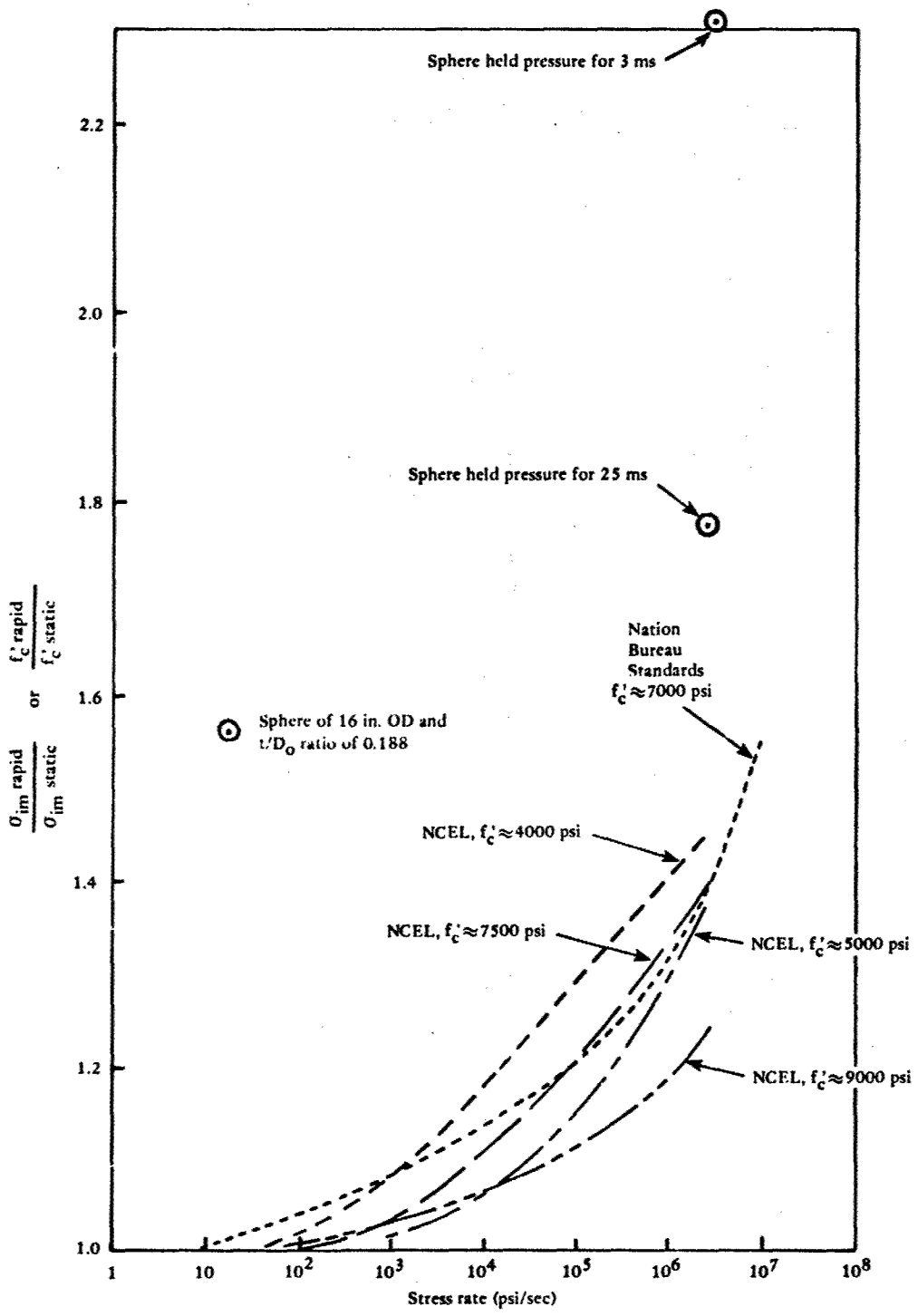

Figure 2.10 Increase in compressive strength as a function of stress rate.

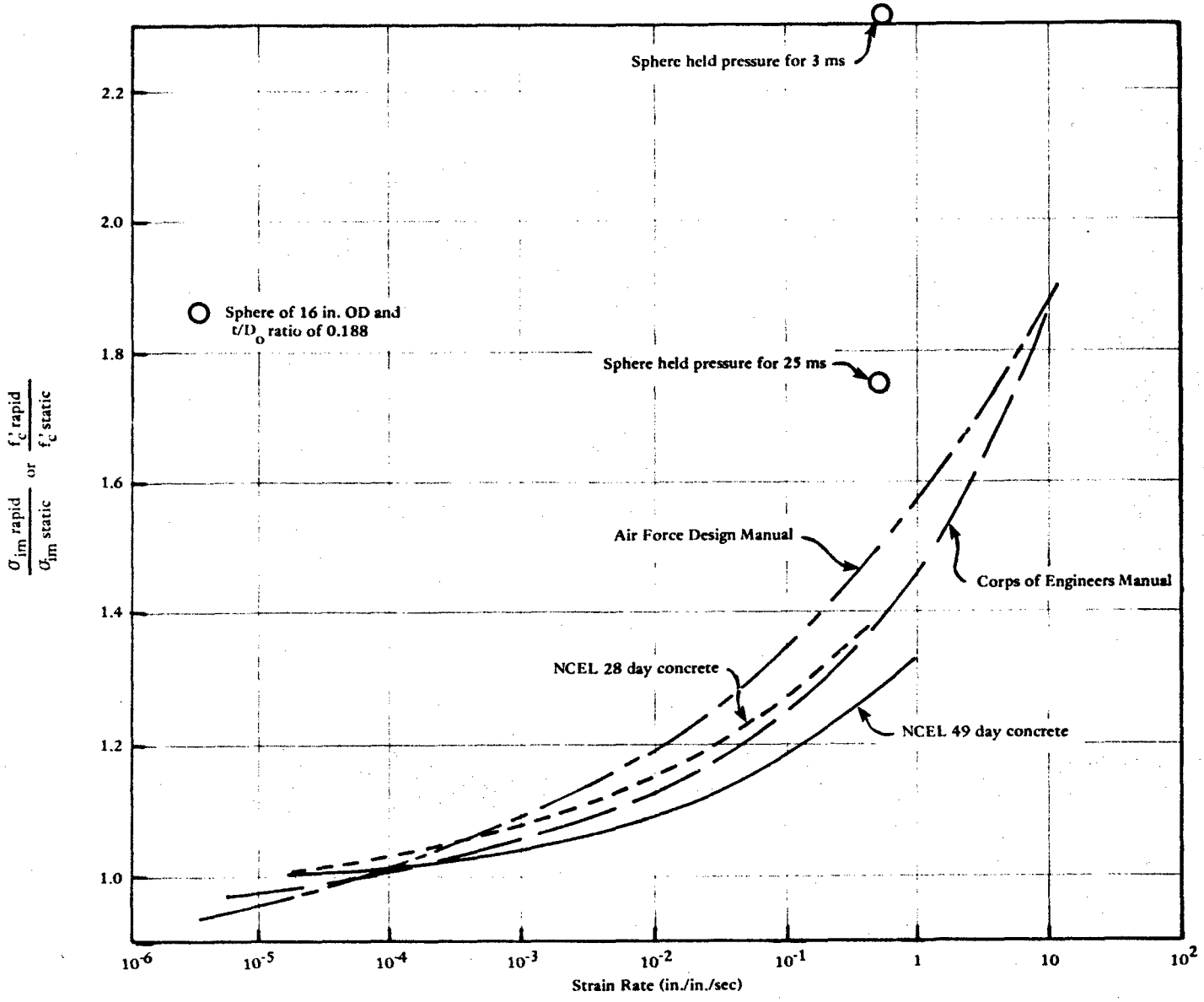

Figure 2.11 Increase in compressive strength as a function of strain rate.

reinforcement have not been investigated, but in general terms the findings from the spherical studies should be applicable.

The first study was on spheres reinforced with steel liners on the inside, on the outside, and on both the inside and outside surfaces (Ref 11). Figure 2.12 shows the 16-inch OD models, which had a t/D_o of 0.063 (for the concrete wall). The quantity of reinforcement varied from 1.8 to 24% by concrete cross-sectional area. Figure 2.13 shows the results of the test program. The implosion strength of the reinforced spheres is presented as the strength relative to that of plain concrete spheres. For a given percentage of steel reinforcement, a liner on both the inside and outside surfaces produced better strength results than if a thicker liner were placed in either the inside or the outside surface.

To substantially increase the implosion strength of concrete spheres required high percentages of reinforcement. For the condition of a liner both on the inside and outside surfaces, a percentage of 12% by area increased the implosion pressure of a plain concrete sphere by a factor of 2.2. On a full-scale structure a percentage of 12% results in thick steel plate. For a 12-foot OD sphere with a t/D_o ratio of 0.063, the thickness of the plate would be about 2.75 inches for a 150,000 psi yield strength steel, which is not a practical design approach.

A more conventional reinforcing scheme was investigated in the second study (Ref 37). Spheres of 32 inches OD with a t/D_o ratio of 0.085 were fabricated with modeled, conventional reinforcing steel cages with percentages of 0.44 and 1.10% by cross-sectional area. Figure 2.14 shows the rebar cage for the higher steel percentage. Implosion results showed that the reinforced spheres failed at relative pressures 5% lower than those for the unreinforced spheres. Near implosion, the interior concrete cover delaminated from the rebar cage. This delamination was not observed for plain concrete spheres of the same wall thickness. The reinforced spheres were fabricated from two hemispheres, and the delamination cracks started at the equatorial joints.

On a full-scale structure, joints would probably not be a problem; however, increases in implosion strength are not anticipated unless the compression steel is tied against lateral movement. Various codes of practice (e.g., Ref 38) require reinforcement be tied if the effect of

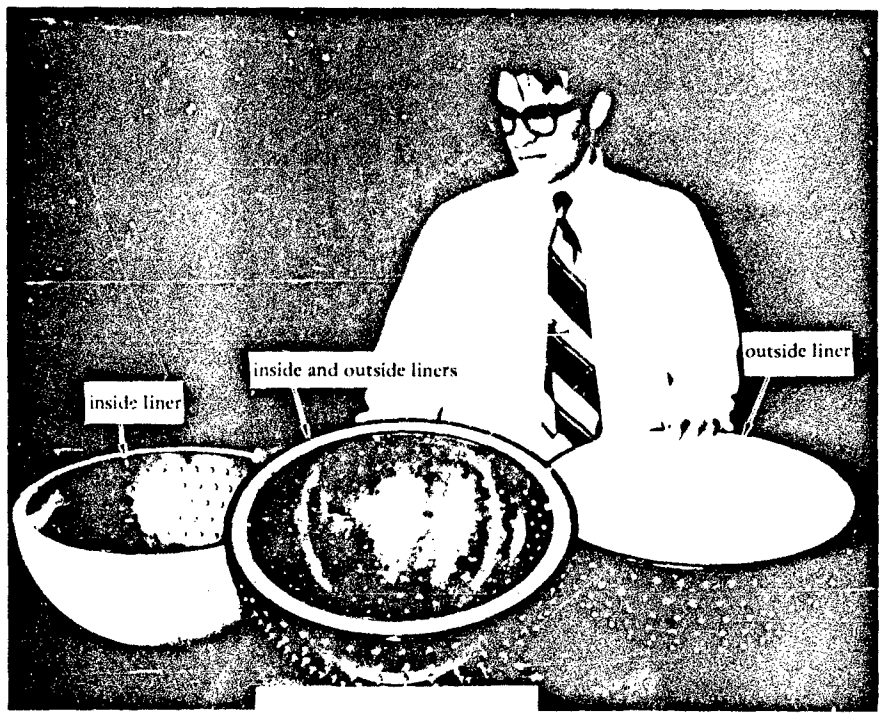

Figure 2.12 Hemisphere sections of steel-lined reinforced concrete spheres. The control (unreinforced) concrete sphere had a $t/D_o = 0.063$.

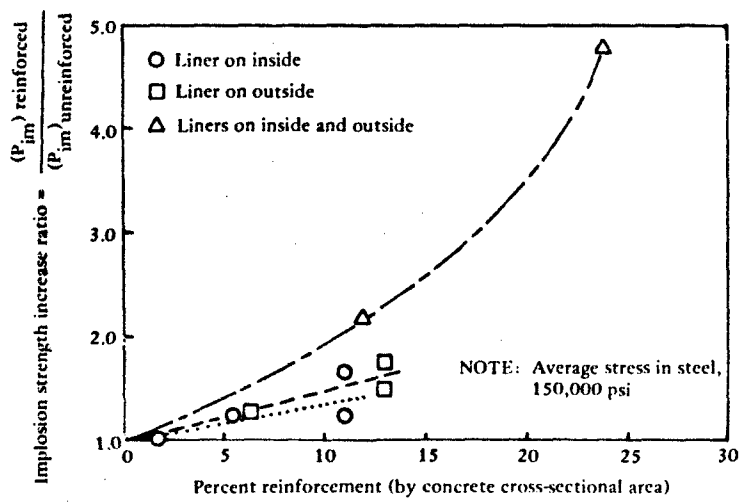

Figure 2.13 The effect of steel-liner reinforcement on the implosion pressure (P_{im}) of thick-walled concrete spheres.

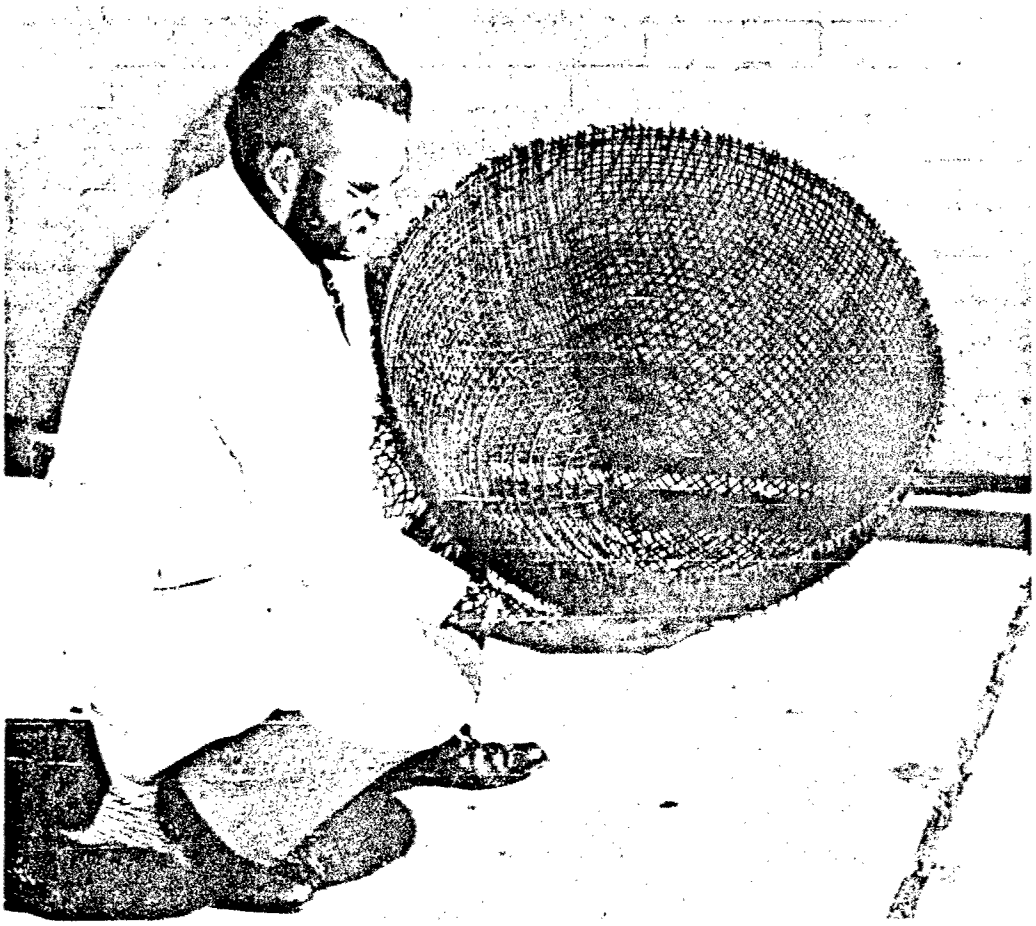

Figure 2.14 Reinforcing cage representing 1.1% steel by area for a concrete sphere of 32-inch OD by 2.71-inch wall thickness.

the reinforcement is to contribute to the strength of a compression member. At operational loads, untied reinforcement will assist in resisting bending displacements caused by out-of-roundness; but, at near failure conditions the untied reinforcement can not be counted on to increase the implosion strength. Hence, when compression reinforcement is not tied, then the member is designed as unreinforced concrete.

The third study was on steel fiber-reinforced-concrete spheres of 16-inch OD, 3-inch wall thickness, and a t/D_o ratio of 0.188 (Ref 39 and 30). Straight steel fibers, 1.5 inches long by 0.017 inch in diameter, were randomly distributed in the concrete at a percentage of 1.5% by volume. The purpose of this study was to investigate cyclic loading effects as discussed earlier. We were also able to compare the static loading strength of three fiber-reinforced spheres to plain concrete spheres of identical size and similar uniaxial concrete compressive strengths. The fiber-reinforced-concrete spheres showed implosion strengths were greater than the plain concrete spheres by a factor of 1.59. This is a substantial increase in implosion strength for a steel reinforcement percentage of only 1.5% by area.

Caution needs to be mentioned regarding steel fiber reinforcement for hydrostatically loaded structures until additional tests can be conducted. A fourth sphere containing steel fiber reinforcement showed an anomalous failure at a pressure 8% lower than plain concrete spheres, a small hole about 1/2 inch in diameter was pushed through the 3-inch thick wall. Perhaps fibers were missing from this region, or perhaps a fiber ball was located in this region.

A somewhat similar failure occurred for a large fiber-reinforced-concrete sphere, 72 inches OD and t/D_o of 0.167 (Ref 40). The reinforcement percentage was 1.5% by area. This sphere was part of an underground blast test program conducted by the Defense Nuclear Agency. After the underground test, which did damage the sphere, the sphere was tested under cyclic hydrostatic loading in a pressure vessel. The failure mode was a 12-inch diameter hole pushed through the 12-inch thick wall in a manner similar to the anomalous failure of the 16-inch OD sphere.

Full-scale concrete structures will require steel reinforcement to resist strains from thermal and shrinkage conditions, loads during construction and transportation stages, moments from discontinuities and out-of-roundness deviations, and other factors. A minimum reinforcement percentage of 0.20% by area should be used.

2.5 EPOXY ADHESIVE JOINTS

Model undersea concrete structures for most of the test programs were fabricated by joining structural components together with an epoxy adhesive. For spheres, two hemispheres were bonded together; for cylinders, end-closures were bonded to the cylinder section. The joints did not appear harmful to the overall behavior. Typically, the initiation of failure did not involve the joints.

The construction approach of bonding elements together was used to bond the hemispherical end closures to a 10-foot diameter by 10-foot long cyclinder as shown in Figure 2.15 (Ref 14). The completed structure, which is shown in the Frontispiece, was submerged for 10.5 months at 600 feet and then returned to land. The joints appeared in excellent condition. After being on land for 4.2 years, the structure was again lowered into the ocean, this time to obtain its implosion strength which occurred at 4,700-foot depth. Again, the joints performed well.

When using epoxy adhesives the American Concrete Institute's guidelines (Ref 41) should be considered. Also the manufacturer's recommended practice should be followed. However, not all commercially available epoxy adhesives for concrete perform equally well. In particular, from tests on a number of epoxy materials, it was found that the bond strength for certain epoxies is damaged by the presence of water (Ref 42). Therefore, before using an epoxy for undersea structural applications, bond strength must be determined by tests on concrete elements bonded in a dry (or damp or wet) condition and then subsequently saturated under pressure.

Water-jetting or sand-blasting is required to roughen the concrete's surfaces. The thickness of the epoxy in the joint should be

less than 1/8 inch. For the joint shown in Figure 2.15, the gap between the mating surfaces was less than 1/8 inch for about 75% of the contact area.

2.6 PENETRATIONS

Tests have shown that concrete spherical structures can have small and even relatively large hull penetrations without reducing implosion strength (Ref 2). The recommended design approach is to use a hull penetration having a rigidity equal to or greater than the rigidity of the concrete removed, and having a mating surface between the concrete and the penetration at a spherical angle (taper to the center of the sphere).

This approach was used for large hull penetrations, which represented 40% of the diameter of the hemispheres, that capped the 10-foot OD cylinder described above (Figure 2.16) (Ref 14). The strains in the concrete near the penetrations did not show an increase over that of other locations during the 10.5-month long ocean test at 600 feet. This, however, could have been due to the low stress levels in the wall (approximately 0.2 f'_c).

For full-scale structures under construction, temporary holes are sometimes required for access to the interior. It is recommended that the edge of the penetration hole have an angle that is tapered to the center of the sphere; or, if that is not possible, the edge should be tapered at an angle that limits shear stresses across the shell thickness to allowable levels. Keyways or ledges around the periphery of the penetration hole should not be used. If concrete is used to fill the hole, then the material should be non-shrinking and have a compressive strength and elastic modulus that is equal to or greater than the concrete in the hull.

Large penetrations in cylindrical hulls have not been investigated. A detailed theoretical analysis using finite elements and a proper constitutive material model for the concrete will produce meaningful results if a large penetration must be located in the cylinder portion

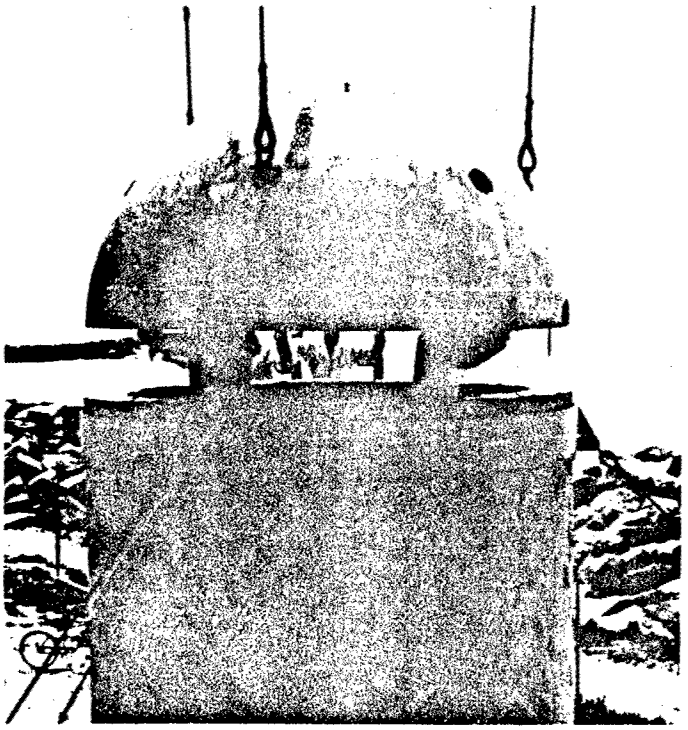

Figure 2.15 Cylindrical structure fabricated by epoxy bonding hemisphere end-closures to cylinder section.

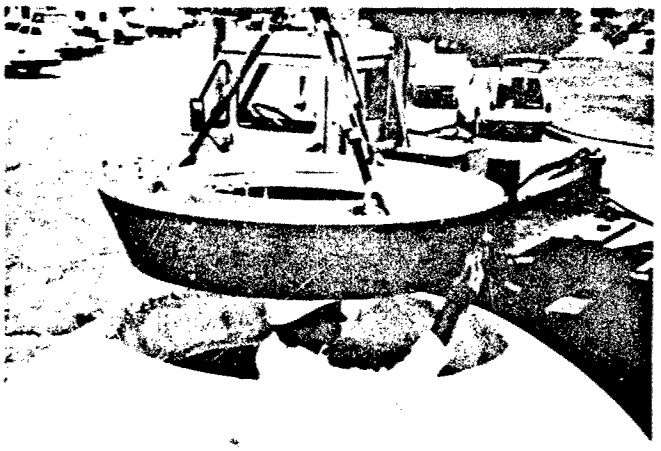

Figure 2.16 Hull penetration in hemisphere end-closure of cylindrical structure represents 40% of the outside diameter of the cylinder.

of the structure. It is preferable, however, to place any large penetrations in the end closures rather than in the wall of the cylinder.

2.7 FACTORS OF SAFETY

The design equations presented in this document to predict implosion pressures of cylindrical and spherical structures require the addition of factors of safety. Factors of safety are applied according to how the structure is to be used.

Different codes of practice have different approaches to assigning factors of safety; however, whatever the approach, the overall factor of safety usually equates to about 2.5 for concrete members under compressive loads (Ref 38 and 43).

The factor of safety is frequently divided into two partial factors: the load factor and the material factor. Without discussing the various codes of practice, these partial factors have the values of about 1.7 for the load factor and about 1.5 for the material factor, and thus, when these factors are multiplied together, the overall factor of safety is approximately 2.5. The load factor accounts for inaccuracies in defining loads, inaccuracies in the design method, variations in construction tolerances, and the importance of the structure (cost and lives involved), and its required reliability. The material factor accounts for variations in concrete strength within the structure and between laboratory and field conditions.

The material factor seldom varies. For undersea structures that are constructed on land or while afloat and then submerged, a material factor of 1.5 is appropriate. If the structure were constructed on the seafloor by tremie placement of concrete, a larger material factor would be warranted. As a guide for the load factor of undersea structures, the value can range from 1.7, if people are not inside the structure, to 2.0 or more if people are inside.

In summary, an overall factor of safety of about 2.5 is proposed for structures that function without people inside and about 3.0, as a minimum, for structures with people inside.

CHAPTER 3. CYLINDRICAL STRUCTURES

Several design approaches are appropriate for cylindrical structures because different geometric configurations behave differently. Analysis methods are presented for thick-walled cylinders, moderately long thin-walled cylinders, and long thin-walled cylinders.

Experimental data exist for each of the geometries. In total, 58 cylinders were tested: 42 had a 16-inch OD (Ref 5, 8, and 12), 15 had a 54-inch OD (Ref 16 and 44), and one had a 121-inch OD (Ref 45). The larger cylinders of 54- and 121-inch diameters generated data of more meaningful quality, probably because they were less sensitive to experimental error. Regardless, data from all clyinder sizes were used in developing the design equations.

The 16-inch OD cylinders are shown in Figure 3.1. These cylinders had various wall thickness-to-diameter, t/D_o, ratios and various length-to-diameter, L/D_o, ratios, so that the wide range of geometric conditions was covered. For the most part, the cylinders were capped with concrete hemispheres of wall thickness equal to that of the cylinder. The concrete uniaxial compressive strengths ranged from 6,000 to 11,000 psi. In general the concrete mix proportions were a water-to-cement ratio between 0.55 and 0.65, an aggregate-to-cement ratio of 3.30, and a cement content of 806 lb/yd^3. Type II Portland cement was used. The maximum size of aggregate passed the No. 4 sieve, which means that, technically, the cylinders were cast of mortar (or microconcrete) rather than a concrete mix.

One of the 54-inch OD cylinders is shown in Figure 3.2. These cylinders also had various t/D_o ratios so they ranged from thin- to thick-walled cylinders. Although all of these cylinders had lengths of 134 inches, the two different end conditions (simple-support and free-support) produced test specimens in the "moderately long" (Figure 3.3)

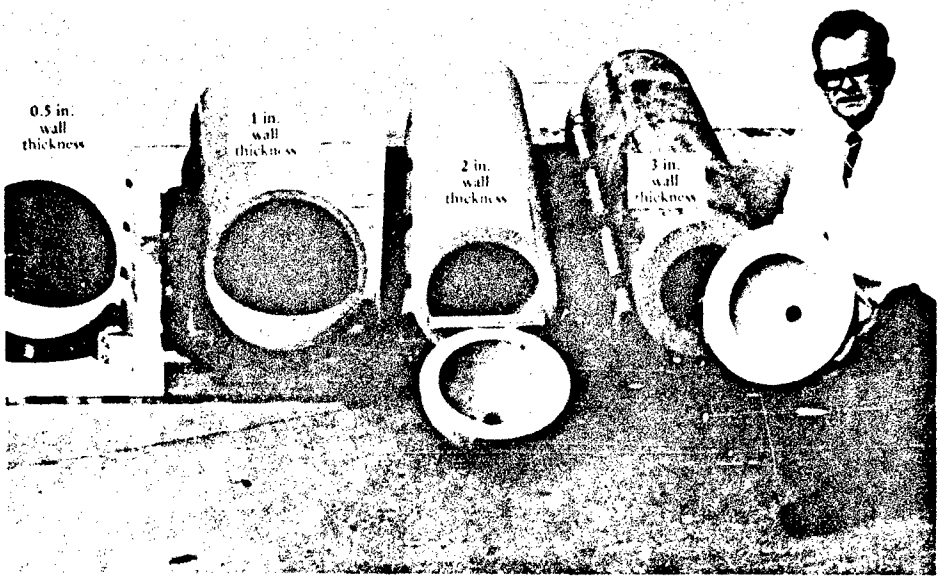

Figure 3.1 16-inch OD concrete test cylinders with various wall thicknesses were tested under hydrostatic loads to implosion.

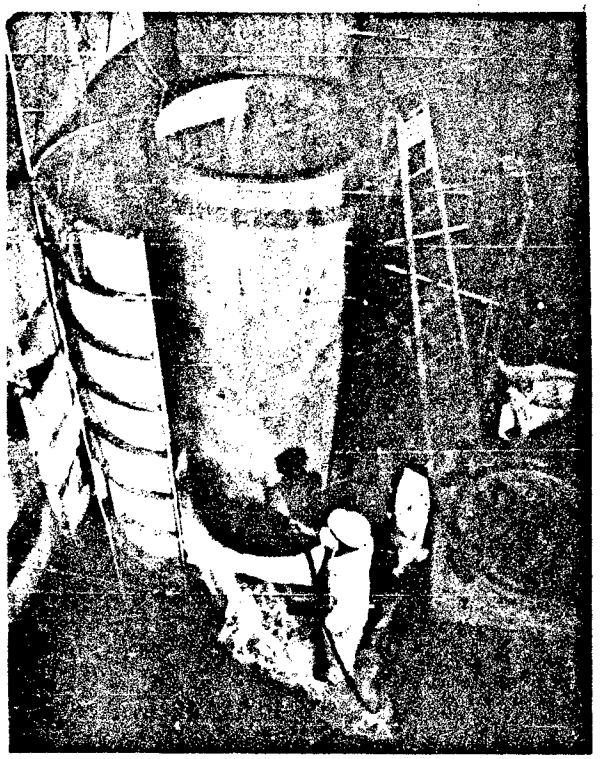

Figure 3.2 54-inch OD concrete test cylinder. For this series of tests walls were 1.31, 1.97, and 3.39 inches thick.

and "long" thin-walled cylinder categories from the point of view of structural analysis. The concrete uniaxial compressive strengths ranged between nominal 6,500 and 9,500 psi. The mix porportions were a water-to- cement ratio of 0.55, a cement-to-sand-to-aggregate proportion of 1:1.96:2.22, and cement content of 676 lb/yd^3. Type II Portland cement was used and the maximum size aggregate was 3/8 inch.

The largest size cylinder, which is shown in the frontispiece and Figure 2.10, was 121 inches OD, 9-1/2-inch wall thickness, and 10 feet long. Thus, the t/D_o ratio was 0.079 and L/D_o was 1.0. The cylinder contained steel reinforcement of 0.70% by area in the hoop direction and in the axial direction. The end closures were concrete hemispheres of wall thickness equal to that of the cylinder. The concrete uniaxial compressive strength was 10,470 psi. The concrete mix proportions were a water-to-cement ratio of 0.40, a cement-to-sand-to-aggregate proportion of 1:1.40:2.50 and a cement content of 734 lb/yd^3. Type II Portland cement was used and the maximum size aggregate was 3/4 inch.

Details of test procedures and test results are reported in the appropriate references. Only those data relevant to developing the design approaches are shown herein (Ref 16).

3.1 THICK-WALLED CYLINDERS

The design approach for predicting implosion of thick-walled cylinders is based on material failure of the cylinder wall. Near implosion, the inelastic behavior of concrete along with time-dependent behavior, such as creep, creates a hoop stress distribution across the wall that is modeled more closely by a uniform stress distribution than by an elastic (Lamé) stress distribution. Uniform hoop stress distribution at implosion is expressed by:

$$\sigma_{im} = P_{im}\left(\frac{R_o}{t}\right) \qquad (3.1)$$

Figure 3.3(a) Post-implosion view of cylinder.

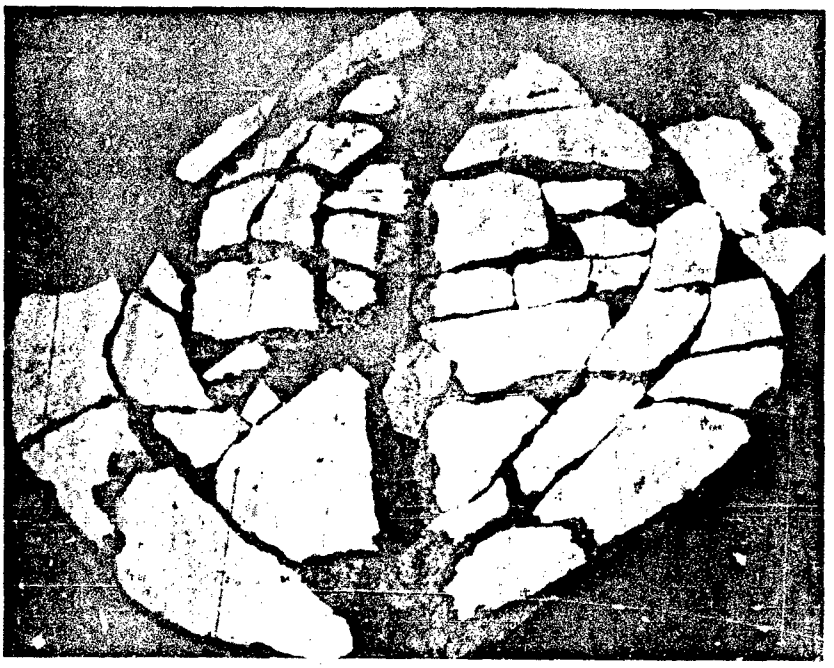

Figure 3.3(b) Fragments of concrete from failure zone.

where: σ_{im} = average hoop stress in the wall at implosion

P_{im} = implosion pressure

R_o = outside radius of the cylinder

t = average wall thickness

The hoop stress at implosion, σ_{im}, can be expressed as the uniaxial compressive strength of concrete multiplied by a strength factor.

$$\sigma_{im} = k_c \; f'_c \tag{3.2}$$

where: k_c = strength factor in the circumferential direction for cylinder structures under hydrostatic loading

f'_c = uniaxial compressive strength of concrete

The term k_c was determined empirically. Figure 3.4 shows k_c as a function of length-to-outside-diameter ratio, L/D_o, for cylinders of various wall-thickness-to-outside-diameter ratio, t/D_o.

For cylinders under external hydrostatic loading, the wall is under biaxial compressive stresses on the inside surface and triaxial compressive stresses at all other locations. The major principal stresses are in the hoop and axial directions, where the hoop stress is about twice the magnitude of the axial stress. The minor principal stress acts radially. If the concrete is considered biaxially loaded, then the hoop-to-axial-stress ratio of 2 increases the compressive strength of concrete by a factor of about 1.25 f'_c (Ref 46). Therefore, k_c values for the cylinders of this program should show a value on the order of 1.25. As a minimum, k_c should be 1.0.

Figure 3.4 shows that short cylinders, those of $L/D_o < 1$, had a k_c arcund 1.25. However, longer cylinders showed a k_c on the order of 1.0.

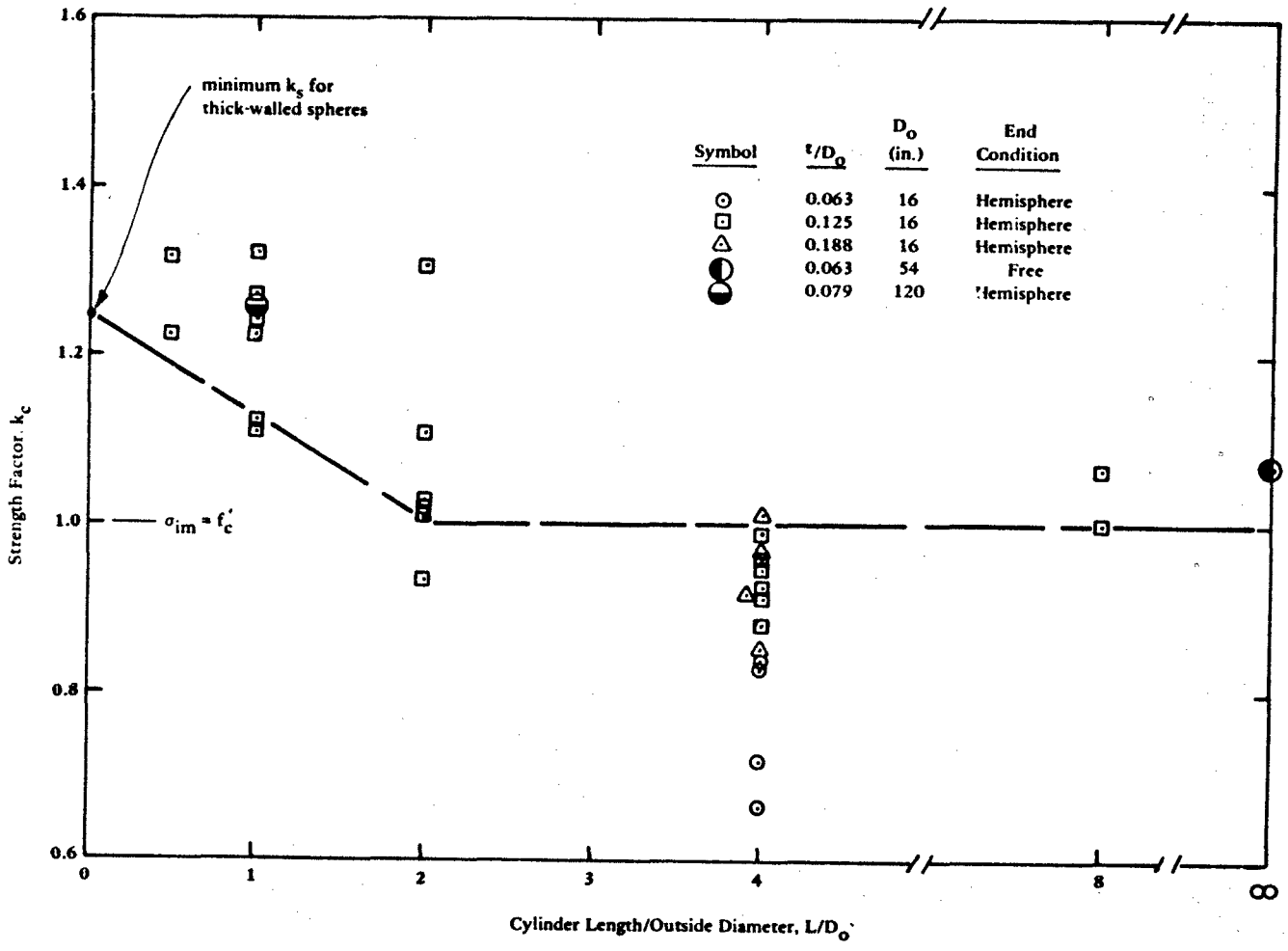

Figure 3.4 Relationship between k_c and L/D_o for thick-walled cylinders.

A decrease in k_c below 1.0 is attributed to an imperfection in the cylinder. An average k_c value of 0.89 was observed at $L/D_o = 4$.*

For design purposes, a $k_c = 1.0$ was selected for cylinders of $L/D_o > 2$. The reader is reminded that this k_c includes the effect of out-of-roundness and experimental error. The reduction in k_c from 1.25 to 1.0, a 20% change, is difficult to assign solely to out-of-roundness effect because thick-walled structures are usually insensitive to small geometric out-of-roundness. The 16-inch OD specimens had the out-of-roundness parameters given in Table 3.1. The specific magnitude of the

Table 3.1. Out-of-Roundness Parameters for 16-Inch OD Cylinders

t/D_o	$\Delta t_{min}/t$	$\Delta R_i/t$	$\Delta R_o/t$
0.03[a]	0.12	0.12	0.12
0.06[b]	0.06	0.06	0.06
0.13[b]	0.03	0.03	0.03
0.19[c]	0.02	0.02	0.02

[a]Thin-walled cylinder.

[b]Border between thin- and thick-walled cylinder.

[c]Thick-walled cylinder.

*Much attention was given to why k_c should be as low as 0.89. If out-of-roundness were the sole cause, then the cylinders showed a decrease in strength of 29% due to out-of-roundness; which is too large an effect for thick-walled cylinders. There is no reason based on engineering mechanics to cause the reduced strength. Some problem related to the fabrication or testing must have been responsible for the low strengths. One procedure that was distinctly different for cylinders with an L/D_o of 4 and 8 was the interior mold. The interior mold was made in segments having a length of $L/D_o = 2$. Cylinders longer than L/D_o of 2 used multiple segments, and it was quite difficult to disassemble the multiple segments to extract the interior mold. If damage was done to the cylinders during this operation, it was not recognized at the time.

out-of-roundness effect could not be determined from the test program; however, the empirical k_c value accounts for whatever out-of-roundness effect that existed. Hence, $k_c = 1.0$ should be a conservative strength factor for design purposes.

Substituting Equation 3.2 into Equation 3.1 and using $R_o = D_o/2$ gives the expression to predict implosion pressure for thick-walled cylinders:

$$P_{im} = 2\, k_c\, f'_c\, (t/D_o) \qquad (3.3)$$

where: $k_c = 1.25 - 0.12\,(L/D_o)$ for $(L/D_o) < 2$

$k_c = 1.0$ for $(L/D_o) \geq 2$

Equation 3.3 is shown in Figure 3.5, and is labeled "thick-walled cylinders." Enter the cylinder's L/D_o and t/D_o on the chart to obtain the P_{im}/f'_c ratio. The implosion pressure, P_{im}, can then be calculated by assuming a concrete compressive strength, f'_c.

The effect of different types of end closures on the implosion strength of thick-walled cylinders is small (Ref 8) so this parameter was not included in Equation 3.3.

3.2 THIN-WALLED CYLINDERS

Thin-walled cylinders are divided into two categories: moderately long cylinders and long cylinders. Moderately long cylinders are influenced by end closures that restrain the cylinder from instability failure. Long cylinders are not influenced by end closures and behave as infinitely long cylinders.

The basis for the design approach was to use Donnell's buckling equation for moderately long cylinders (Ref 47) and Bresse's equation for long cylinders (Ref 48). Both equations predict the hoop stresses in the wall of the cylinder at buckling.

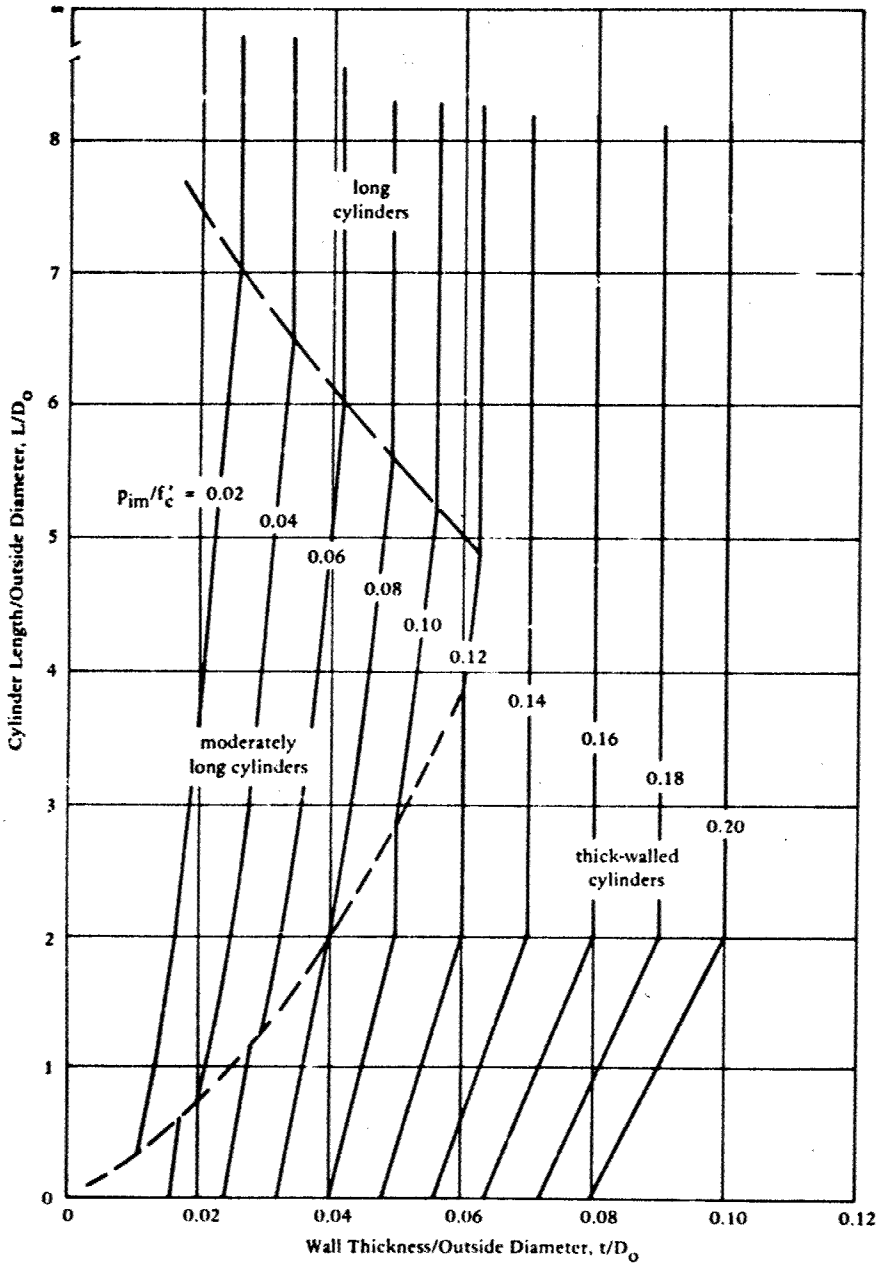

Figure 3.5 Design guide for predicting implosion pressure of concrete cylinder structures.

Note: Enter the chart with known or assumed values for the cylinder's L/D_o and t/D_o ratios to find the P_{im}/f'_c ratio. Select a compressive strength (known or assumed) between 6,000 and 10,000 psi and calculate P_{im}.

Donnell's Equation

$$(\sigma_{im})_D = \frac{0.855\ E_c}{(1-\nu^2)^{3/4}} \left(\frac{t}{R}\right)^{3/2} \frac{R}{L} \eta \qquad (3.4)$$

where: $(\sigma_{im})_D$ = hoop stress in cylinder wall at implosion, predicted by Donnell's equation

E_c = concrete elastic modulus, psi

L = uninterrupted length of cylinder, in.

R = mean radius, in.

t = wall thickness, in.

η = plasticity reduction factor

ν = Poisson's ratio

and

Bresse's Equation

$$(\sigma_{im})_B = \frac{E_c}{4\ (1-\nu^2)} \left(\frac{t}{R}\right)^2 \eta \qquad (3.5)$$

where: $(\sigma_{im})_B$ = hoop stress in cylinder wall at implosion, predicted by Bresse's equation

Using $\nu = 0.20$ and the approximation $R = D_o/2$, Donnell's equation becomes:

$$(\sigma_{im})_D = \frac{1.25\ E_c\ \eta \left(\frac{t}{D_o}\right)^{1.5}}{L/D_o} \qquad (3.6)$$

and Bresse' equation

$$(\sigma_{im})_B = 1.04\ E_c\ \eta \left(\frac{t}{D_o}\right)^2 \qquad (3.7)$$

The elastic condition exists when $\eta = 1$.

Figure 3.6 shows the experimental data of the elastic moduli as a function of compressive strength for the concrete used in the 54-inch OD

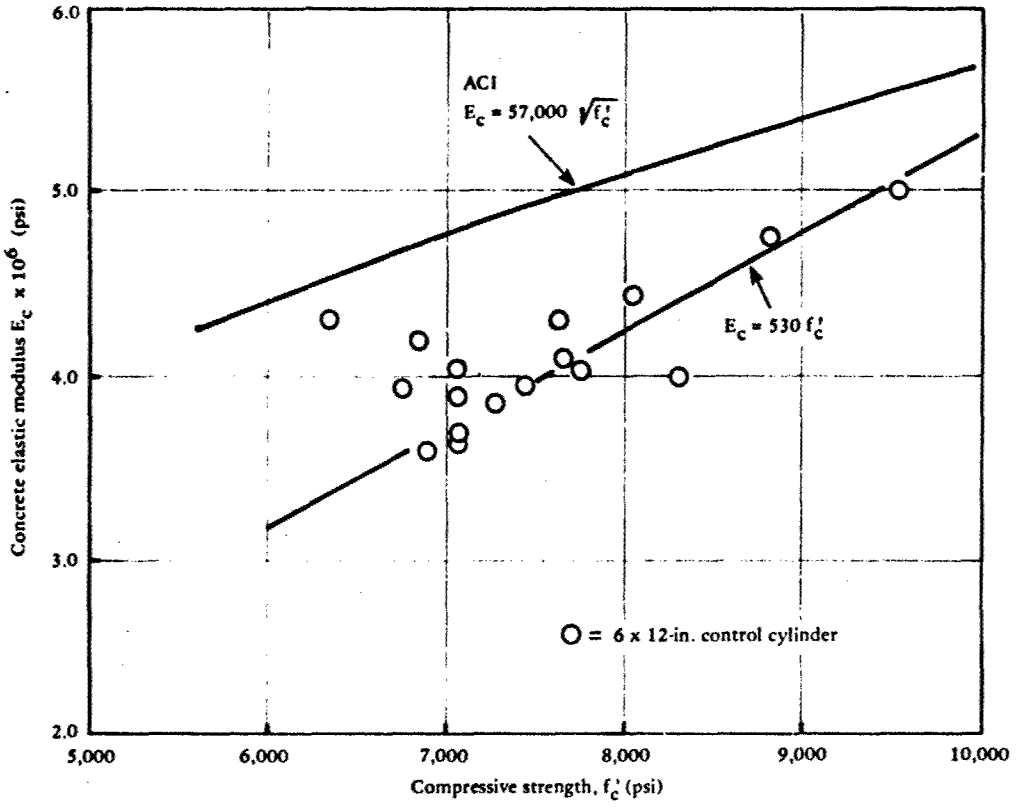

Figure 3.6 Concrete elastic modulus values (obtained as secant modulus up to 0.4 f'_c) of 54 - inch OD cylinders.

cylinder tests specimens. E_c was obtained experimentally as the secant of the uniaxial compressive stress-strain curves from the beginning up to 40% of ultimate strength. From these data the following empirical expression was developed to predict E_c for concretes in the compressive strength range of 6,000 to 10,000 psi.

$$E_c = 530\, f'_c \qquad 6{,}000 \text{ psi} < f'_c < 10{,}000 \text{ psi}^* \tag{3.8}$$

The American Concrete Institute (ACI) expression for elastic modulus (Ref 39) is shown in Figure 3.6 for comparision. The ACI expression is known to over estimate E_c for high strength concretes (Ref 49).

Equations 3.6 and 3.7 predict the elastic hoop stress at implosion when the plasticity reduction factor, η, is 1.0. When η is less than 1.0, its primary function is to account for inelastic material behavior as E_c deviates from elastic response. For the thin-walled cylinder design approach, η is used in a broader manner. It is the empirical factor to relate Donnell's and Bresse's equations to the test results. Thus η represents more than just inelastic material behavior; it also includes the effects of cylinder out-of-roundness, experimental error, and theoretical equation limitations.

Empirical values were calculated by dividing the experimental hoop stress at implosion (assuming a uniform stress distribution across the wall) by the elastic hoop stress at buckling, Equation 3.6 or 3.7. As the t/D_o ratio increases for thin-walled cylinders, and the failure mode enters the transition region from buckling to material failure, greater inelastic material effects occur and η becomes smaller. This is seen in Figures 3.7, 3.8, and 3.9.

These data are shown in Figure 3.10 where η is a function of the stress level in the cylinder wall at implosion. The fitted inelastic buckling curves of Figures 3.7 and 3.8 were transferred to Figure 3.10

*Outside this range, Equation 3.8 becomes inaccurate, underestimating E_c below 6,000 psi and overestimating E_c above 10,000 psi (Ref 16).

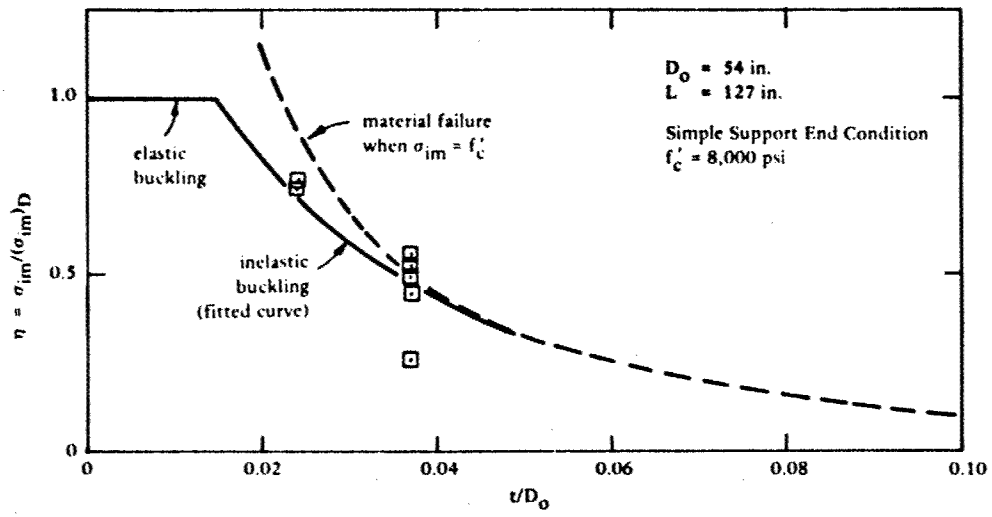

Figure 3.7 Implosion of moderately long cylinders with D_o = 54 inches.

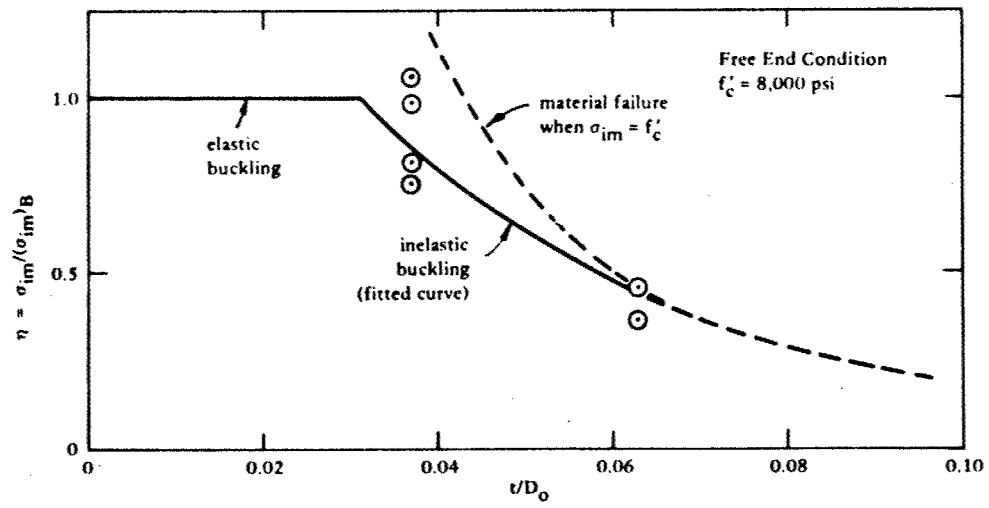

Figure 3.8 Implosion of long cylinders with D_o = 54 inches.

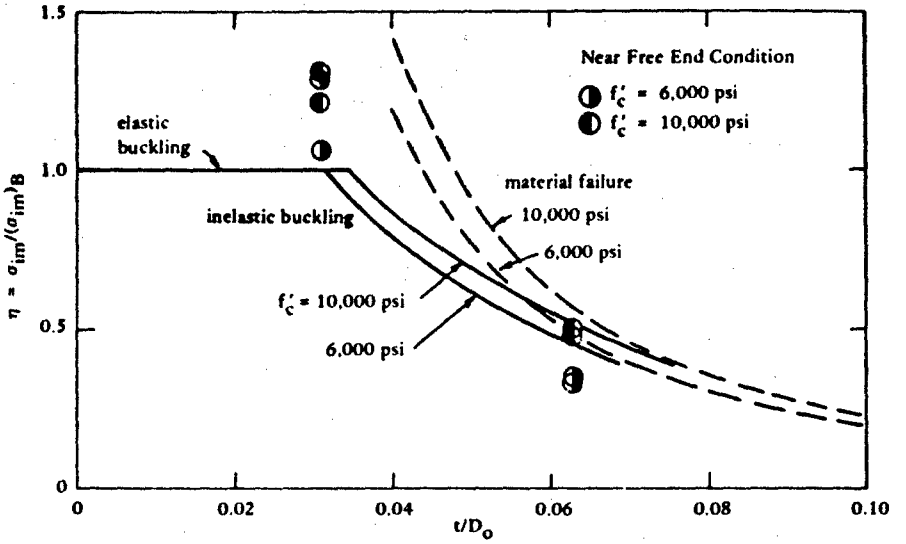

Figure 3.9 Implosion of long cylinders with D_o = 16 inch (after Ref. 12).

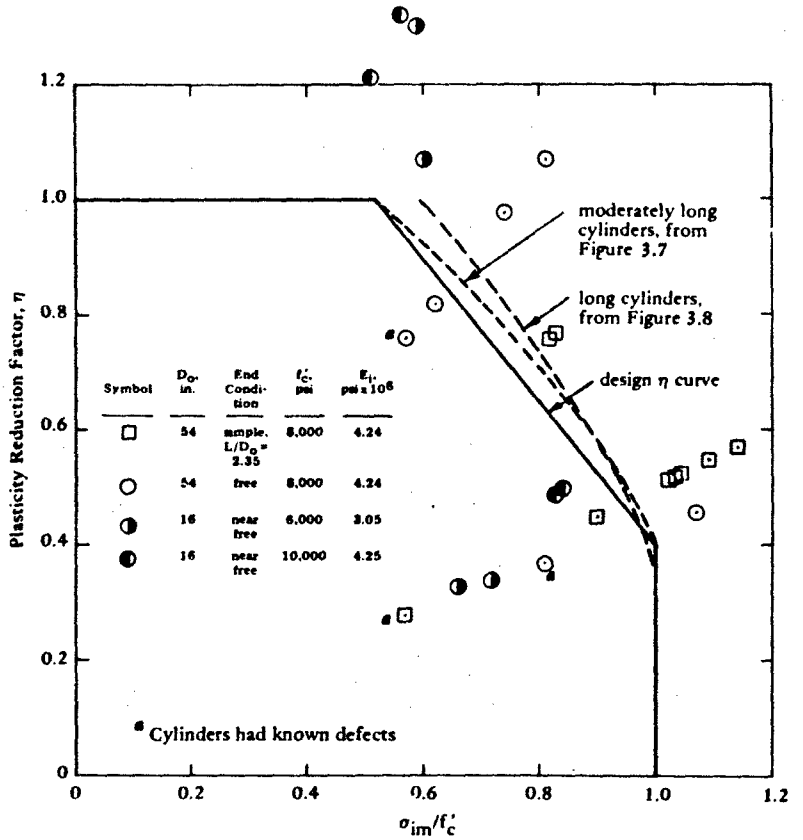

Figure 3.10 Plasticity reduction factor as a function of stress level in cylinder wall at implosion.

and then a design η curve was selected which was applicable to both moderately long and long cylinders. The η expression is:

$$\eta = 1.65 - 1.25\left(\frac{\sigma_{im}}{f'_c}\right) \qquad 0.52 < \frac{\sigma_{im}}{f'_c} < 1.0 \tag{3.9}$$

3.2.1 Moderately-Long Cylinders

The expression to predict implosion pressure for moderately long cylinders was developed as follows.

Equations 3.8 and 3.9 are substituted into Donnell's simplified, equation, Equation 3.6, to yield:

$$\frac{\sigma_{im}}{f'_c} = \frac{1{,}090\left(\frac{t}{D_o}\right)^{1.5}}{\frac{L}{D_o} + 830\left(\frac{t}{D_o}\right)^{1.5}} \tag{3.10}$$

The stress level at implosion, σ_{im}/f'_c, is calculated by knowing the geometry of the cylinder structure. After calculating σ_{im}/f'_c, the following conditions determine the next step:

a. If $\sigma_{im}/f'_c > 1.0$, a thick-wall analysis is used to predict implosion (Equation 3.3).

b. If $0.52 < \sigma_{im}/f'_c < 1.0$, then η is calculated by Equation 3.9.

c. If $\sigma_{im}/f'_c < 0.52$, then $\eta = 1.0$.

If steps (b) or (c) control, the following expression, which predicts the implosion pressure, is used. Equations 3.6 and 3.8 are substituted into Equation 3.1 to obtain:

$$P_{im} = \frac{1{,}320\ \eta\ f'_c\ \left(\frac{t}{D_o}\right)^{2.5}}{\frac{L}{D_o}} \qquad (3.11)$$

A design chart approach is given in Figure 3.5. Enter the cylinder's L/D_o and t/D_o ratios on the chart to determine the P_{im}/f'_c ratio. The structure is assumed to have a simple support end condition.

For the case of fixed support end conditions, it has been shown analytically (Ref 50) that a 6% implosion strength increase can be expected.

3.2.2 Long Cylinders

The expressions to predict implosion pressure for long cylinders were developed as follows.

Equations 3.8 and 3.9 are substituted into the simplified Bresse's equation, Equation 3.7, to yield:

$$\frac{\sigma_{im}}{f'_c} = \frac{910\left(\frac{t}{D_o}\right)^2}{1 + 690\left(\frac{t}{D_o}\right)^2} \qquad (3.12)$$

Once the stress level at implosion is calculated, the same conditions for moderately long cylinders hold; that is:

a. If $\sigma_{im}/f'_c > 1.0$, a thick-wall analysis is used to predict implosion (Equation 3.3).

b. If $0.52 < \sigma_{im}/f'_c < 1.0$, then η is calculated by Equation 3.9.

c. If $\sigma_{im}/f'_c < 0.52$, then $\eta = 1.0$.

If steps (b) or (c) control, the following expression, which was developed by substituting Equations 3.7 and 3.8 into Equation 3.1, predicts the implosion pressure:

$$P_{im} = 1{,}100\ \eta\ f'_c \left(\frac{t}{D_o}\right)^3 \qquad (3.13)$$

A design chart approach is given in Figure 3.5. Enter the structure's L/D_o and t/D_o ratio on the chart to determine the P_{im}/f'_c ratio.

3.2.3 Out-of-Roundness

The design chart in Figure 3.5 was developed from theoretical equations that were modified by empirical data. The empirical data were from specimens that had geometric out-of-roundness.

For the 54-inch OD cylinders (Ref 16 and 44), the geometry was extensively measured to define initial out-of-roundness. A summary of the out-of-roundness parameters is given in Table 3.2. This information, however, does not give the complete picture because the location of the thinnest wall thickness coincided with the location of largest radius deviation (or flat spot). Figures 3.11 and 3.12 show the initial geometry. The worst flat spot location was caused by a seam in the exterior casting mold. Displacement recordings taken on the cylinders during hydrostatic loading tests showed that the failure occurred at the worst flat spot location.

Table 3.2. Out-of-Roundness Parameters for 54-Inch OD Cylinders

t/D_o	Out-of-Roundness Parameters		
	$\Delta t_{min}/t$	$\Delta R_i/t$	$\Delta R_o/t$
0.024	0.08	0.04	0.10
0.037	0.06	0.03	0.06
0.063	0.04	0.02	0.03

NOTE: Radius deviations are for radii less than the nominal radii.

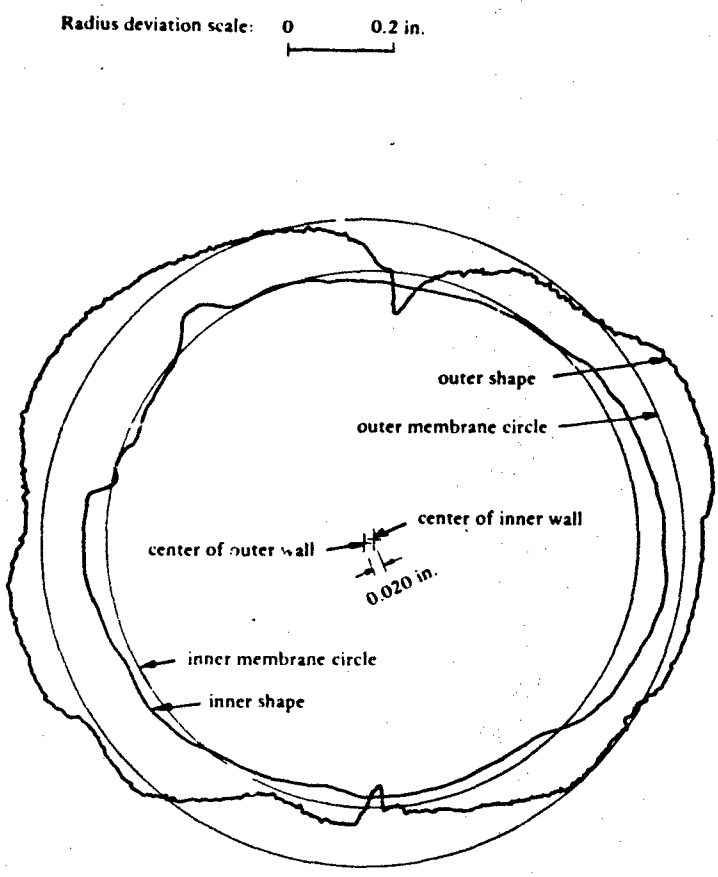

Figure 3.11 Initial cross-section shape showing relative changes in wall thickness and flat spots for a 54 inch OD cylinder having a t/D_o ratio of 0.037.

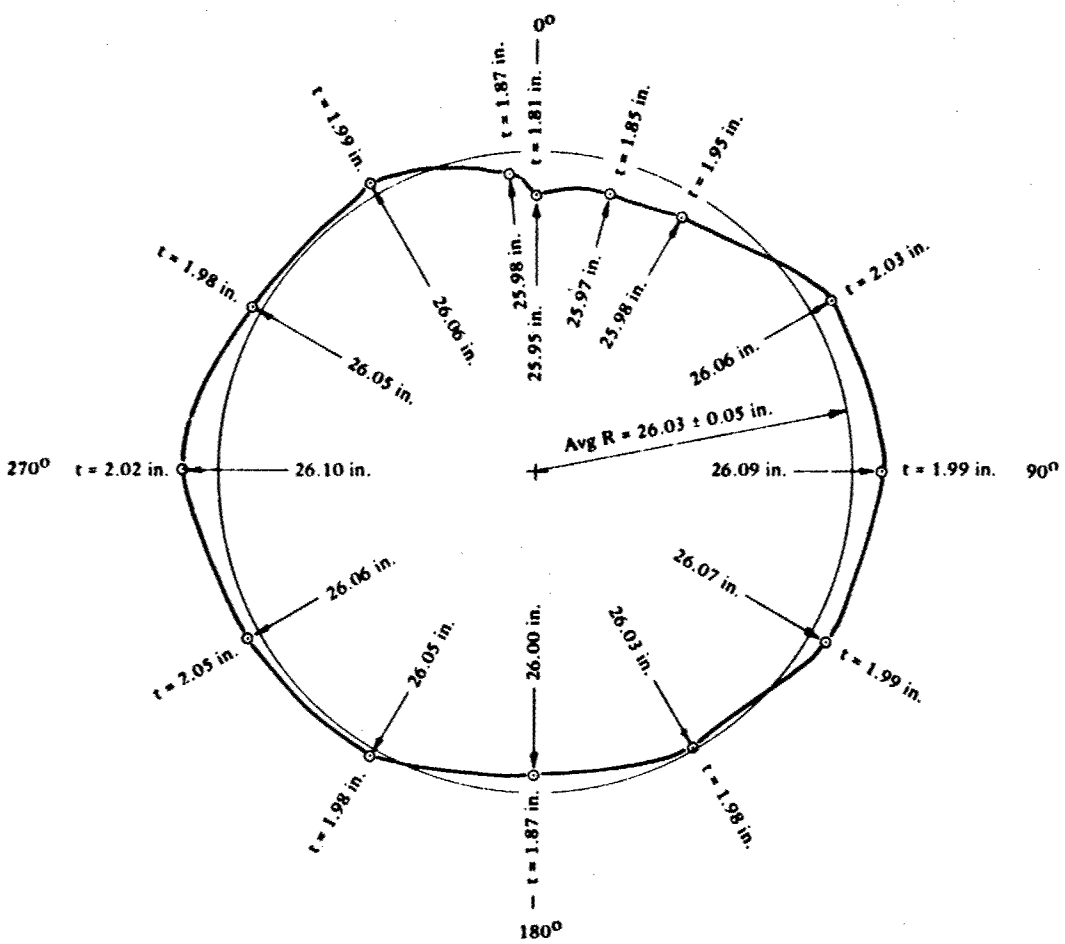

Figure 3.12 Variation in values of wall thickness and mean radius as an average of 54 inch OD cylinders of t/D_o ratio of 0.037.

For full-scale structures, out-of-roundness tolerances can be maintained that are better than those in Table 3.2; therefore, the design chart of Figure 3.5 should be conservative in predicting implosion, in regard to influences from out-of-roundness.

Certain geometries of thin-walled cyliners are more sensitive to axial load effects than other geometries. The curvature parameter, Z, helps to qualitatively define which geometries are sensitive to out-of-roundness deviations (Ref 47).

$$Z = \frac{L^2 \sqrt{1 - \nu^2}}{R\, t}$$

For concrete, ν is about 0.20 and $\sqrt{1-\nu^2}$ is approximately 1.0 and thus

$$Z = \frac{L^2}{R\, t} \qquad (3.14)$$

Under hydrostatic loading conditions, cylinders having Z greater than 100 are not sensitive to "normal" deviations in roundness. The out-of-roundness parameters given in Table 3.2 are considered within the limits of "normal" deviations. However, cylinders with Z less than 100 are sensitive to out-of-roundness, and detailed finite element analyses should be performed on those design cases.

3.3 DESIGN EXAMPLE, CYLINDRICAL STRUCTURE

A 100-foot OD, 200-foot long cylindrical structure, which will not be manned, is oriented vertically on the the seafloor at a depth of 500 feet. Hemispheres cap the ends of the cylinder. Seawater ballast fills the structure to a height of 100 feet. Hence, the maximum applied pressure loading is 400 feet or 178 psi. The wall thickness has been preliminarily selected as 3.5 feet and the concrete strength at time of pressure loading as 7,500 psi.

The first step is to determine whether the structure is a moderately long, a long thin-walled, or a thick-walled cylinder. In Figure 3.5, enter an L/D_o of 2.0 and t/D_o of 0.035 to determine that the structure is a moderately long cylinder.

A quick estimate of the implosion strength can be obtained from Figure 3.5. An approximate P_{im}/f'_c is obtained as 0.067

$$P_{im} = 0.067\ f'_c = 0.067\ (7{,}500\ \text{psi}) = 502\ \text{psi}$$

Using the design equations to estimate P_{im} requires the following steps:

- The stress level at implosion, σ_{im}/f'_c, for a moderately long cylinder is calculated using Equation 3.10.

$$\frac{\sigma_{im}}{f'_c} = \frac{1{,}090\ (0.035)^{1.5}}{2.0 + 830\ (0.035)^{1.5}} = 0.95$$

- When σ_{im}/f'_c is less than 1.0, the plasticity reduction factor, η, is calculated using Equation 3.9.

$$\eta = 1.65 - 1.25\ (0.95) = 0.46$$

- Now use the implosion equation, Equation 3.11:

$$P_{im} = \frac{1{,}320\ (0.46)\ (7{,}500)\ (0.035)^{2.5}}{2.0} = 522\ \text{psi}$$

Note that the design chart estimate and the calculated estimate are in reasonable agreement with each other.

The factor of safety is:

$$\text{F.S.} = \frac{P_{im}}{P_{operational}} = \frac{522}{178} = 2.93$$

For an unmanned structure, a safety factor of 2.93 is greater than the prescribed 2.5, so the design is adequate. The wall thickness could be revised to a smaller t/D_o ratio, or the concrete strength could be reduced so that the final safety factor was 2.5.

Check the curvature parameter, Z. of Equation 3.14 to determine if this structure is sensitive to out-of-roundness deviations.

$$Z = \frac{L^2}{R\,t} = \frac{(200)^2}{48.3\ (3.5)} = 236 > 100$$

Thus the cylinder is not considered sensitive if normal roundness tolerances are maintained during construction.

CHAPTER 4. SPHERICAL STRUCTURES

Design equations to predict the implosion pressure of thick-walled and thin-walled spheres are presented. Only thick-walled spheres have been tested experimentally.

The experimental specimens were mostly 16-inch OD spheres with t/D_o ratios ranging from 0.062 to 0.25, and concrete compressive strengths ranging from 6,000 to 11,000 psi (Ref 1, 2, 3, and 4). Seventeen of these spheres were tested under short-term loading, i.e, each sphere was placed in a laboratory pressure vessel and the pressure steadily increased until the sphere failed by implosion. The implosion results for these spheres are shown in Figure 4.1. The design approach for thick-walled spheres is based primarily on these data. Larger 32-inch (Ref 37) and 66-inch OD spheres (Ref 10) with t/D_o ratios 0.85 and 0.0625, respectively, were also tested to failure by implosion. The results from the larger sphere tests are also included in Figure 4.1.

For the 16- and 32-inch OD spheres the concrete mix porportions were a water-to-cement ratio between 0.56 and 0.65, an aggregate-to-cement ratio of 3.30, and a cement content of 806 lb/yd^3. Type II Portland cement and aggregate passing the No. 4 size sieve were used. For the 66-inch OD spheres, the concrete was manufactured at a local commercial batch plant and transit mixed. The mix proportions were water-to-cement ratio of 0.41, cement-to-sand-to-aggregate proportions of 1:1.85:2.28, and a cement content of 733 lb/yd^3. Type II Portland cement, a maximum size aggregate of 3/4 inch, and a water-reducing admixture were used.

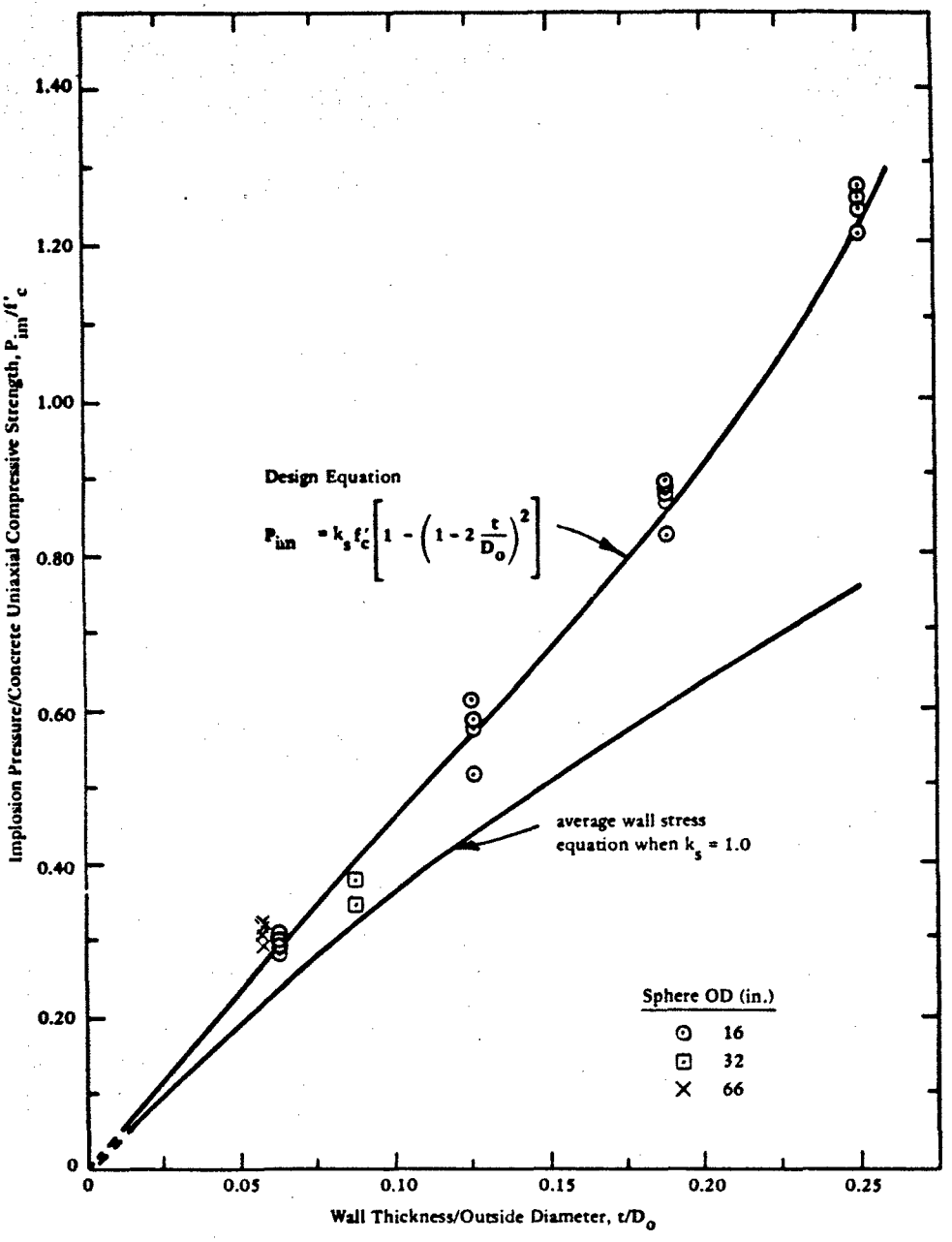

Figure 4.1 Design chart to predict implosion of thick-walled spheres.

4.1 THICK-WALLED SPHERES

The design approach for predicting the implosion pressure of a thick-walled, plain concrete sphere subjected to a uniform external pressure is based on a material failure criterion (not on a buckling failure), viz., the average circumferential ("hoop") compressive stress, σ_{im}, in the sphere wall at the time of implosion of the sphere. The average wall stress is used because, at or near failure, the inelastic behavior of concrete causes redistribution of stresses across the wall thickness. The average hoop stress in the wall of a sphere at implosion due to external pressure can be expressed as:

$$\sigma_{im} = \frac{P_{im}}{1 - \left(1-2\,\frac{t}{D_o}\right)^2} \qquad (4.1)$$

where: σ_{im} = average wall hoop stress at implosion, psi

P_{im} = implosion pressure, psi

t/D_o = wall thickness to OD ratio

Since the sphere wall is in a state of multi-axial compressive stress, σ_{im} should be greater than the uniaxial compressive strength, f'_c, of the concrete. This was confirmed by the implosion tests as shown in Figure 4.1. The empirically determined difference between σ_{im} and f'_c is defined as a design strength factor, k_s, for spherical structures.

$$\sigma_{im} = k_s\, f'_c \qquad (4.2)$$

Figure 4.2 shows k_s as a function of t/D_o ratio. As t/D_o increases, k_s increases exponentially. This is understandable, because as the wall becomes thicker, the state of stress in the wall approaches that of equal triaxial compression. At the limit, when $t/D_o = 0.50$, which is a solid sphere of concrete, the multiaxial state of stress is that of equal triaxial compression, and k_s is a rather large number (say 10 or

100; it's actual value in unknown but it is not infinity). The fitted curve in Figure 4.2 is expressed as:

$$k_s = 1.22 + 0.014\, e^{13.5\,(t/D_o)} \qquad (4.3)$$

To predict implosion of thick-walled spheres, the design equation is obtained by substituting Equation 4.2 into Equation 4.1:

$$P_{im} = k_s\, f'_c \left[1 - \left(1-2\,\frac{t}{D_o}\right)^2\right] \qquad (4.4)$$

Equation 4.4 is shown in Figure 4.1, which may be used as a design chart.

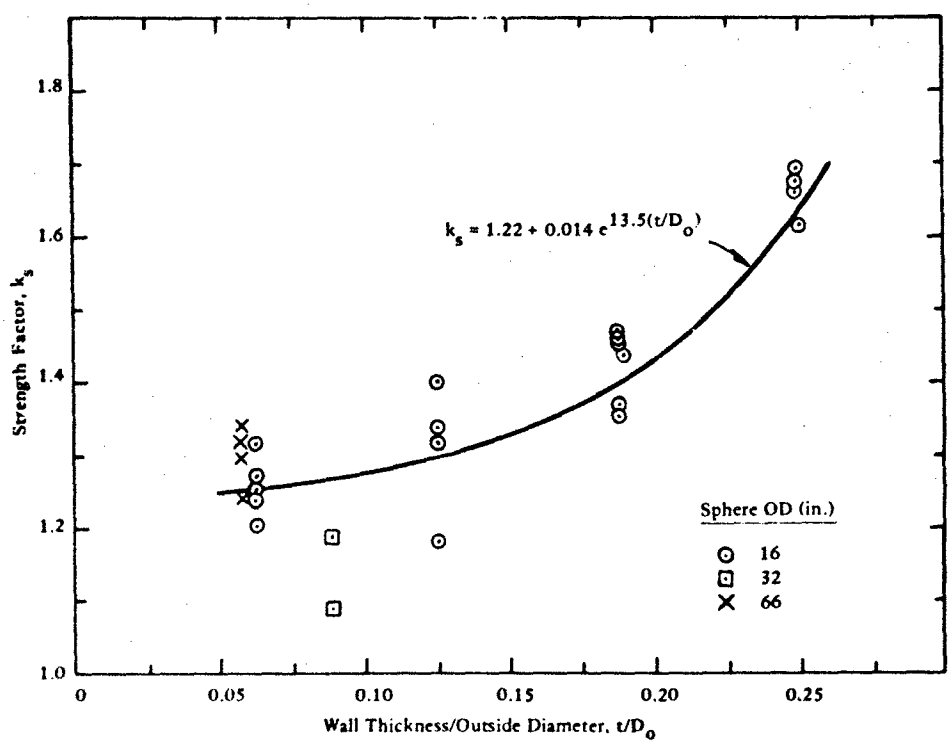

Figure 4.2 Relationship between k_s and t/D_o of thick-walled spheres.

During early work on thick-walled spheres (Ref 4), cracks appeared in the plane of the wall thickness. This cracking was detected before implosion and, therefore, was considered a preliminary failure mode. Two observations were the basis for this proposed failure mode. First, strain gages mounted on the interior of the wall recorded continuously increasing compressive strains until at some pressure the strains started to decrease in magnitude even though the pressure continued to increase; and, second, fragments of imploded spheres having t/D_o ratios of 0.188 and 0.250 showed distinct in-plane or delamination cracks. In addition, theoretical calculations showed that radial strains were in tension and of magnitudes sufficient to cause cracking. Although data were quite limited, an expression was developed to predict the pressure at initiation of in-plane cracking using Lamé's elastic thick-wall theory equation for calculating stresses on the interior wall modified by a strength factor, k_s, of 1.35. The expression applied only to spheres having a t/D_o greater than approximately 0.10.

More recent work (Ref 39 and 40) began to raise doubts about the in-plane cracking concept. At present, an explanation of the earlier findings is:

a. The strain gage readings reduced in magnitude because the concrete surface began to crush. The inside concrete surface was under biaxial loading, while all other concrete was under triaxial loadings, so this surface was most susceptible to crushing. Also, the double curvature of the inside surface assisted in physically holding the concrete in place as it progressed into the descending portion of stress-strain behavior (crushing). The earlier results showed that the strain gages started to record reduced strains at the stress level of 1.35 f'_c. The stress limit for prisms under pure biaxial loading is about 1.25 f'_c; hence, the inside surface of the concrete sphere had likely reached its ultimate limit.

b. The in-plane cracks, probably, did not develop as the pressure loading was applied, but rather as the load was removed abruptly by implosion. Sphere implosion was sudden; the shock forces at failure combined with the rapid load removal caused tensile microcracks to join into distinct in-plane cracks. Tensile strains existed in the radial direction, and the direction of tensile microcracks would have been parallel to the wall surfaces, or in-plane to the wall surfaces.

To summarize, in-plane cracks are probably not a preliminary failure mode for thick-walled spheres. Rather, the past expression to predict in-plane cracks could be considered to predict the pressure at initiation of crushing of concrete on the inside surface. Crushing does not mean disintegrating or spalling, only that the descending portion of stress-strain behavior has been entered for the biaxially loaded concrete. This expression is:

$$P_{bi} = 0.90\, f'_c \left[1 - \left(1-2\frac{t}{D_o}\right)^3\right], \text{ for } \frac{t}{D_o} \geq 0.10 \qquad (4.5)$$

where: P_{bi} = pressure at initiation of crushing of biaxially loaded concrete on inside surface of sphere, psi

Equation 4.5 is shown in Figure 4.3.

4.2 THIN-WALLED SPHERES

Since data were not available on thin-walled spheres, past literature was reviewed for a conservative expression for buckling of spheres. Buchert (Ref 51) applied the following equation, which is adapted herein:

$$P_{im} = 0.18\, E_c\, \eta \left(\frac{t}{R}\right)^2 \qquad (4.6)$$

where: E_c = concrete modulus of elasticity, psi

R = mean radius, inch

η = plasticity reduction factor

t = wall thickness, inch

The constant in Equation 4.6 is 15% of the constant in the theoretical elastic buckling expression for spheres; however, it is well known that the elastic buckling pressure is unobtainable by physical models. The reduced constant in Equation 4.6 makes the expression practical.

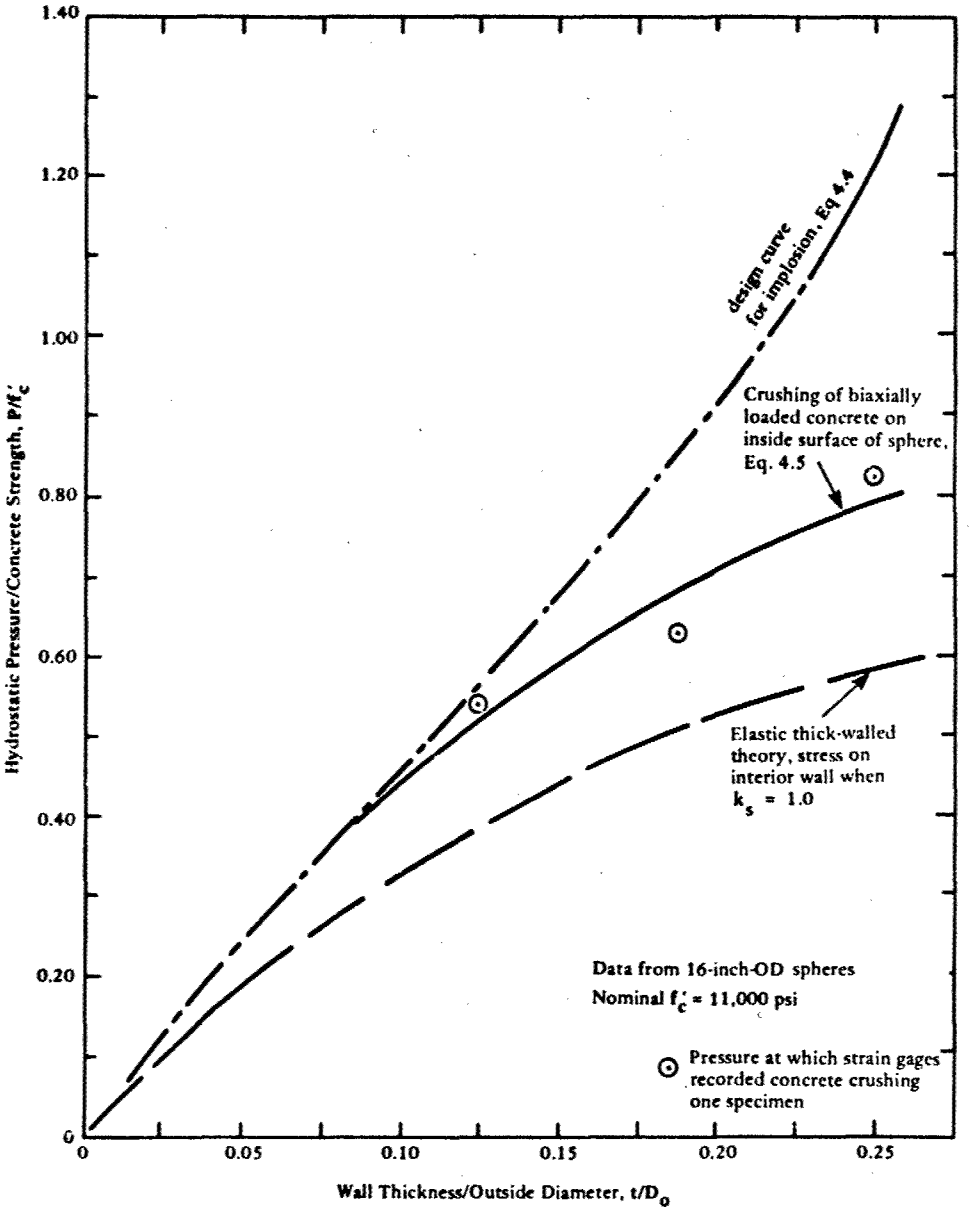

Figure 4.3 Experimental data that indicate the initiation of concrete crushing on the interior surface of thick-walled spheres.

For simplicity, it was assumed that the plasticity reduction factor was the minimum obtained for thin-walled cylinders, $\eta = 0.40$. As t/D_o ratios become smaller, spheres exhibit less inelastic behavior, so η should increase; however the sphere's sensitivity to out-of-roundness will increase. Hence, a conservative approach is to use a consistent η of 0.40. (Note that this is a significant reduction in the value of the plasticity factor ($\eta = 0.70$) recommended in the first edition of this handbook and, therefore, will lead to a more conservative design.)

Also, in a manner similar to that used for the thin-walled cylinders, the empirical expression for concrete modulus of elasticity, $E_c = 530\ f'_c$, and the approximation of $R = D_o/2$ are introduced. The design equation to predict implosion for thin-walled spheres thus becomes:

$$P_{im} = 152\ f'_c \left(\frac{t}{D_o}\right)^2 \qquad (4.7)$$

where: $\frac{t}{D_o} < 0.033$, and $6{,}000 < f'_c < 10{,}000$ psi

Figure 4.4, which shows the curve for Equation 4.7, may be used as a design chart.

4.3 DESIGN EXAMPLE, SPHERICAL STRUCTURE

A 100-foot OD spherical structure is required for temporary manned occupation at the 2,000-foot depth in the ocean. Installation procedures require that the structure have a positive buoyancy of about 300 tons.

The following design procedure will determine the concrete compressive strength and sphere wall thickness to meet the above requirements. The reader is cautioned, however, that the buoyancy problem is quite complicated due to water absorption of the concrete,

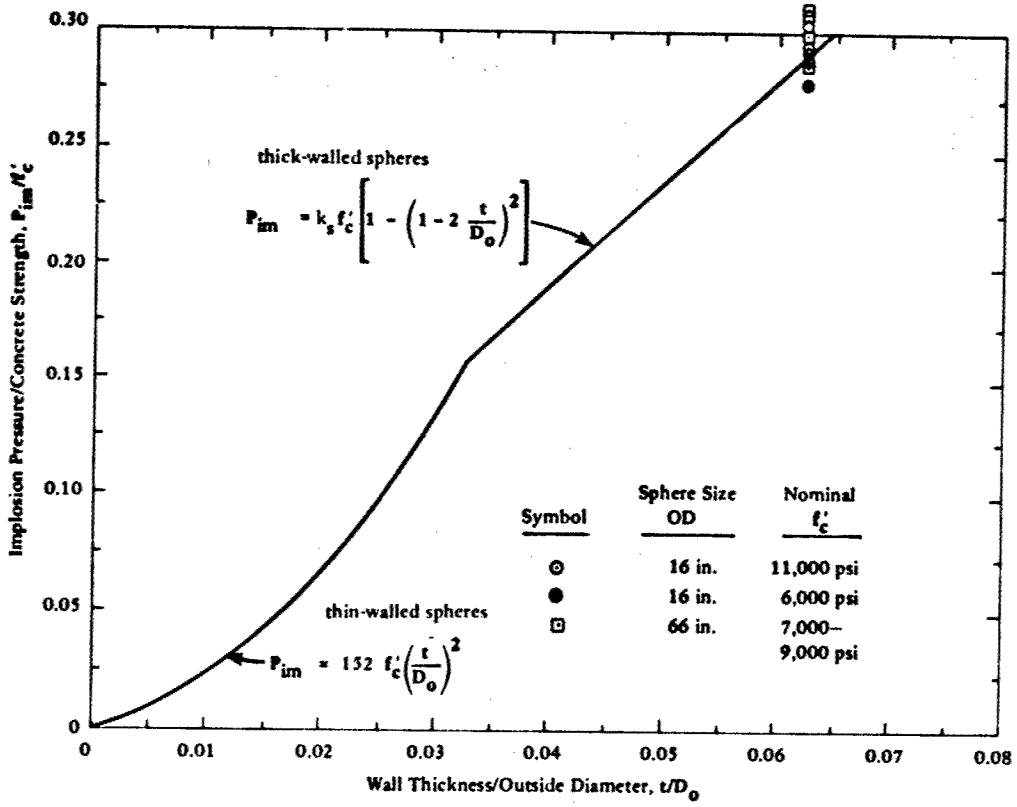

Figure 4.4 Implosion of thin-walled and thick-walled spheres. Experimental data is not available for spheres with a $t/D_o < 0.062$.

volume change of the sphere under load, density changes of the concrete, and other factors. This example will, simplistically, assume a constant 300-ton buoyancy.

The first step is to determine the wall thickness that provides the proper buoyancy for the sphere. Assume that seawater weighs 64 lb/ft^3 and concrete 155 lb/ft^3.

$$\text{(displaced volume)} - \text{(weight of sphere)} = 300 \text{ tons}$$

$$(64 \text{ pcf}) \frac{\pi}{6} (100)^3 - (155 \text{ pcf}) \frac{\pi}{6} \left[(100)^3 - D_i^{\,3}\right] = 600{,}000 \text{ lb}$$

Solving for D_i yields:

$$D_i = 84.08 \text{ ft (inside diameter)}$$

Therefore, $t = (100-84.08)\frac{1}{2} = 7.96$ ft (wall thickness)

and $\frac{t}{D_o} = 0.08$

The second step is to determine the uniaxial compressive strength of the concrete, f'_c, to give the structure an operational depth of 2,000 feet. The operational pressure, P_{op}, is:

$$P_{op} = 2{,}000 \text{ ft } (0.445 \text{ psi/ft}) = 890 \text{ psi}$$

The implosion pressure is:

$$P_{im} = (P_{op})\ (F.S.)$$

where: F.S. = factor of safety

Use a F.S. of 3.0 for a temporarily manned structure.

$$P_{im} = (890)\ (3.0) = 2{,}670 \text{ psi}$$

Use Equation 4.3 to determine k_s and Equation 4.4 to determine f'_c:

$$k_s = 1.22 + 0.014e^{13.5\ (t/D_o)} = 1.27$$

$$f'_c = \frac{P_{im}}{k_s\left[1 - \left(1 - 2\,\frac{t}{D_o}\right)^2\right]}$$

$$f'_c = \frac{2{,}670}{(1.27)\left[1 - (1 - 2 \cdot 0.08)^2\right]} = 7{,}140 \text{ psi}$$

which is the compressive strength required at the age when the structure experiences hydrostatic load.

CHAPTER 5. SUMMARY

Test results from laboratory and ocean investigations conducted at NCEL over the past two decades have been condensed into design guides for undersea, pressure-resistant concrete structures. These guides are principally for designing cylindrical and spherical concrete structures to resist the externally applied pressures of hydrostatic loads and thus be safe from implosion failure. Thin-walled and thick-walled structures are considered.

For predicting implosion pressures of thick-walled cylinders, an empirical expression, Equation 3.3, is presented. For thin-walled cylinders, the cases of moderately long, and long cylinders are treated separately. Buckling expressions by Donnell for moderately long cylinders and by Bresse for long cylinders are simplified by incorporating experimentally verified numerical values for the modulus of elasticity and Poisson's ratio of high strength concrete to obtain the design Equations 3.6 and 3.7. These expressions are then modified by an empirically determined plasticity reduction factor. The plasticity reduction factor is presented as a function of the stress level in the cylinder wall at implosion, Equation 3.9. A combined design guide for thick-walled, moderately long, and long cylinders is presented in a chart format in Figure 3.5.

Implosion pressures for thick-walled spheres can be predicted by Equation 4.4, which is an expression based on the average circumferential compressive stress in the concrete sphere wall at the time of failure by implosion. The wall stress is related to the uniaxial compressive strength of concrete by an empirically derived factor. For thin-walled spheres, a conservative buckling expression, Equation 4.7, can be used.

Conservatism has been used in developing these design guides because the technology for submerged concrete structures is relatively

undeveloped. Many concrete technology topics remain to be investigated, and, for that matter, not all the information presented herein has been completely validated. When judgments were made in developing these design guides, engineering knowledge, past experience with concrete used on land and with steel structures under hydrostatic pressure, were conservatively applied. With future research and field experience it is expected that these guidelines will be improved.

CHAPTER 6. ACKNOWLEDGMENTS

The authors gratefully acknowledge the assistance of Mr. Philip C. Zubiate and Mr. Larry D. Underbakke who were senior engineering technicians during most of the test programs reported herein; their hard work, sustained efforts and imagination were major contributions to the development of pressure-resistant concrete structures. For his perserverance, overall technical guidance and programmatic contributions over the past several years of these investigations, we express our sincere appreciation to Mr. John Freund, Program Manager, Naval Sea Systems Command, Washington, DC.

CHAPTER 7. REFERENCES

1. Naval Civil Engineering Laboratory. Technical Report R-517: Behavior of spherical concrete hulls under hydrostatic loading, Part I. Exploratory investigation, by J.D. Stachiw and K.O. Gray. Port Hueneme, Calif., Mar 1967. (AD 649290)

2. _____. Technical Report R-547: Behavior of spherical concrete hulls under hydrostatic loading, Part II. Effect of penetrations, by J.D. Stachiw. Port Hueneme, Calif., Oct 1967. (AD 661187)

3. _____. Technical Report R-588: Behavior of spherical concrete hulls under hydrostatic loading, Part III. Relationship between thickness-to-diameter ratio and critical pressures, straing, and water permeation rates, by J.D. Stachiw and K. Mack. Port Hueneme, Calif., Jun 1968. (AD 8354926)

4. _____. Technical Report R-679: Failure of thick-walled concrete spheres subjected to hydrostatic loading, by H.H. Haynes and R.A. Hoofnagle. Port Hueneme, Calif., May 1970. (AD 708011)

5. _____. Technical Report R-696: Influence of length-to-diameter ratio on the behavior of concrete cylindrical hulls under hydrostatic loading, by H.H. Haynes and R.J. Ross. Port Hueneme, Calif., Sep 1970. (AD 713088)

6. _____. Technical Report R-673 and R-673S: In-situ strength of subaqueous concrete, by W.R. Lorman. Port Hueneme, Calif., Apr 1971 and Sep 1971. (AD 705993 and AD 889084L)

7. _____. Technical Report R-735: Influence of stiff equatorial rings on concrete spherical hulls subjected to hydrostatic loading, by L.F. Kahn. Port Hueneme, Calif., Aug 1971. (AD 731352)

8. _____. Technical Report R-735: Influence of stiff equatorial rings on concrete spherical hulls subjected to hydrostatic loading, by L.F. Kahn and J.D. Stachiw. Port Hueneme, Calif., Aug 1971. (AD 731352)

9. _____. Technical Report R-753: Polymer-impregnated concrete spherical hulls under hydrostatic loading, by H.H. Haynes and N.D. Albertsen. Port Hueneme, Calif., Dec 1971. (AD 736598)

10. _____. Technical Report R-774: Behavior of 66-inch concrete spheres under short-and long-term hydrostatic loading, by H.H. Haynes and L.F. Kahn. Port Hueneme, Calif., Sep 1972. (AD 748584)

11. _____. Technical Report R-785: Hydrostatic loading of concrete spherical hulls reinforced with steel liners, by H.H. Haynes, G.L. Page, and R.J. Ross. Port Hueneme, Calif., Apr 1973. (AD 759684)

12. _____. Technical Report R-790: Influence of compressive strength and wall thickness on behavior of concrete cylindrical hulls under hydrostatic loading, by N.D. Albertsen. Port Hueneme, Calif., Jun 1973. (AD 764054)

13. _____. Technical Report R-805: Long-term deep-ocean test of concrete spherical structures. Part I: Fabrication, emplacement, and initial inspections, by H.H. Haynes. Port Hueneme, Calif., Mar 1974. (AD 777079)

14. _____. Technical Report R-817: Seafloor construction experiment, SEACON I - An integrated evaluation of seafloor construction equipment and techniques, by T. Kretschmer, et al. Port Hueneme, Calif., Feb 1975. (AD A009097)

15. _____. Technical Report R-869: Long-term, deep-ocean test of concrete spherical structures - Results after 6 years, by H.H. Haynes and R.S. Highberg. Port Hueneme, Calif., Jan 1979. (AD A070864)

16. _____. Technical Report R-874: Design for implosion of concrete cylinder structures under hydrostatic loading, by H.H. Haynes. Port Hueneme, Calif., Aug 1979. (AD A078641)

17. _____. Technical Report R-915: Long-term, deep-ocean test of concrete spherical structures - results after 13 years, by R.D. Rail and R.L. Wendt. Port Hueneme, Calif., July 1985. (A 160232)

18. American Concrete Institute. ACI 357-R: Guide for the design and construction of fixed offshore concrete structures. Revised 1985. ACI Committee 357. Detroit, Michigan.

19. Naval Civil Engineering Laboratory. Technical Note N-1360: SEA CACHE: A mobile petroleum, oils, lubricants (POL) seafloor storage and supply system for advanced bases, by N.D. Albertsen and H.H. Haynes. Port Hueneme, Calif., Nov 1974. (AD A004936)

20. B.C. Gerwick, Jr., W. Webster, D. Smith and J.D. Stachiw. Feasibility study for concrete submarine. University of California, Berkely, Calif., Dec 1974.

21. S. Mindess and J.F. Young. Concrete. Prentice-Hall, Englewood Cliffs, N.J., 1981, pp 422-424.

22. Naval Civil Engineering Laboratory. Technical Note N-1308: Compressive strength of 67-year-old concrete submerged in seawater, by H.H. Haynes and P.C. Zubiate, Port Hueneme, Calif., Oct 1973. (AD 772527)

23. G. Verbeck, "Pore structure," Special Technical Publication No. 169-A, Significance of Test and Properties of Concrete and Concrete Making Materials, American Society of Testing and Materials, Philadelphia, Penn., 1966, pp 211-219.

24. D.D. Double, and A. Hellawell, "The solidification of cement," Scientific American, vol 237, no. 1, Jul 1977, pp 82-90.

25. T.C. Powers, "The nature of concrete," Special Technical Publication No. 169-A, Significance of Tests and Properties of Concrete and Concrete Making Materials, American Society of Testing and Materials, Philadelphia, Penn., 1966, pp 61-72.

26. Naval Civil Engineering Laboratory. Technical Note N-1436: Seawater absorption and compressive strength of concrete at ocean depths, by H.H. Haynes, R.S. Highberg, and B.A. Nordby. Port Hueneme, Calif., Apr 1976. (AD A026192)

27. _____. Technical Note N-1603: Compressive strength of freshly mixed concrete placed, cured, and tested in the deep ocean, by H.H. Haynes and L.D. Underbakke. Port Hueneme, Calif., Feb 1981. (AD B058918L)

28. _____. Technical Memorandum M-44-80-6: Concrete spherical structures subjected to rapid loading by external pressure - an exploratory investigation, by H.H. Haynes. Port Hueneme, Calif., Mar 1980.

29. S. Stockl, "Strength of concrete under uniaxial sustained loading," Concrete for Nuclear Reactors, vol I, ACI Special Publication SP-34, pp 313-326.

30. H.H. Haynes and M.B. Balachandra, "Low-cycle fatigue of fiber reinforced concrete spheres under hydrostatic loading," ACI Special Publication SP-75, Fatigue of Concrete Structures, Sep 1982, pp 289-305.

31. S.S. Takhar, I.J. Jordaan, and B.R. Gamble, "Fatigue of concrete under lateral confining pressure," ACI Special Publication SP-41, Fatigue of Concrete, 1973, pp 59-69.

32. M.E. Awad, and H.K. Hilsdorf, "Strength and deformation characteristics of plain concrete subject to high repeated and sustained loads," ACI Special Publication SP-41, Fatigue of Concrete, 1973, pp 1-13.

33. Naval Civil Engineering Laboratory. Technical Report R-447, Dynamic properties of plain Portland cement concrete, by W.L. Cowell, Port Hueneme, Calif., Jun 1966.

34. U.S. National Bureau of Standards. Report 1523: The Effect of loading rate on the compressive strength and elastic properties of plain concrete by D. Watstein and A.P. Boresi. Washington D.C., Mar 1952.

35. U.S. Army Corps of Engineers. Engineering Manual EM-1110-345-414: Engineering and design: Design of structures to resist the effects of atomic weapons. Washington D.C., Mar 1957.

36. U.S. Air Force Special Weapons Center. Technical Document Report Number AFSWC-TDR-62-138: Air Force design manual: Principles and practices for design of hardened structures. Kirtland Air Force Base, N.M., Dec 1962.

37. Naval Civil Engineering Laboratory. Technical Note N-1364: Behavior of steel bar reinforced concrete spheres under hydrostatic loading, by N.D. Albertsen. Port Hueneme, Calif., Apr 1975. (AD A011810)

38. American Concrete Institute. ACI 318: Building code requirements for reinforced concrete, Detroit, Mi., 1983.

39. Naval Civil Engineering Laboratory. Technical Memorandum M-44-78-03: Test results from repeated hydrostatic loading of thick-walled concrete spheres, by P.C. Zubiate, Jr. and H.H. Haynes. Port Hueneme, Calif., Nov 1977.

40. _____. Technical Memorandum M-44-77-08: Data from hydrostatic test of concrete sphere AY-11, by H.H. Haynes and P.C. Zubiate, Jr. Port Hueneme, Calif., May 1977.

41. American Concrete Institute. ACI 503R: "Use of epoxy compounds with concrete," Detroit, Mi., 1980

42. Naval Civil Engineering Laboratory. Technical Note N-1173: Evaluation of eight epoxy adhesives for bonding concrete and micro-concrete structural components exposed to room and to hydrostatic pressure conditions, by T. Roe, A.F. Curry, and P.C. Zubiate. Port Hueneme, Calif., Jul 1971. (AD 888505L)

43. Federation Internationale de la Precontrainte (FIP), Recommendations for the design and construction of concrete sea structures, 3rd edition, London, England, 1977.

44. Naval Civil Engineering Laboratory. Technical Memorandum M-44-76-04: Results of concrete cylinder implosion test program, by H.H. Haynes and R.S. Highberg. Port Hueneme, Calif., Apr 1976.

45. R.S. Highberg and H.H. Haynes. "Ocean implosion test of concrete (SEACON) cylindrical structure," paper presented at Proceedings of the Offshore Technology Conference, Houston, Texas, May 1977. (OTC Paper No. 3011)

46. H. Kupfer, H.K. Hilsdorf, and H. Rusch. "Behavior of concrete under biaxial loading," ACI, vol 66, no. 8, Aug 1969, pp 656-666.

47. National Advisory Committee for Aeronautics, Langley Research Center. Report No. 874: A simplified method of elastic stability analysis for thin cylindrical shells, by S.B. Batdorf. Jun 1947, pp 285-309.

48. S.P. Timoshenko and J.M. Gere. Theory of elastic stability. 2nd ed., New York, N.Y., McGraw-Hill Book Company, Inc., 1961, p 293.

49. ACI Committee 363: State-of-the-art report on high strength concrete, Journal of ACI, Jul-Aug 1984, pp 364-411.

50. O. Olsen, "Implosion analysis of concrete cylinders under hydrostatic pressure," ACI, vol 75, no. 3, Mar 1973, pp 82-85.

51. K.P. Buchert. Buckling of shell and shell-like structures. K.P. Buchert and Associates, Columbia, Mo., 1973.

CHAPTER 8. NOMENCLATURE

D_i	Inside diameter (ft or in.)
D_o	Outside diameter (ft or in.)
e_D	Diameter deviation (ft or in.)
e_t	Wall thickness deviation (ft or in.)
E_c	Modulus of elasticity of concrete (psi)
f'_c	Uniaxial compressive strength of concrete (psi)
k_c	Strength increase factor in hoop direction for cylinders
k_s	Strength increase factor for spheres
L	Uninterrupted length of cylinder (ft or in.)
P	Hydrostatic pressure (psi)
P_{bi}	Pressure at initiation of crushing on inside wall of sphere (psi)
P_{im}	Implosion pressure (psi)
P_{op}	Operational pressure (psi)
P_{pl}	Initiation of in-plane cracking pressure (psi)
P_s	Sustained pressure (psi)
R	Mean radius (ft or in.)
R_i	Inside radius of cylinder (ft or in.)
R_o	Outside radius of cylinder (ft or in.)
F.S.	Factor of Safety
t	Wall thickness (ft or in.)
Z	Curvature parameter
β	End condition factor
λ	Long-term loading factor

γ_f Partial load factor

γ_{mc} Partial material factor for concrete

η Plasticity reduction factor

θ Length-to-diameter factor

ν Poisson's ratio

σ_{im} Average stress in hoop direction of cylinder or sphere wall at implosion (psi)

σ Stress in concrete (psi)

DISTRIBUTION LIST

ARMY BMDSC-RE (H McClellan), Huntsville, AL
ARMY CRREL Library, Hanover, NH
ARMY EWES Library, Vicksburg MS
BUREAU OF RECLAMATION J Graham, Denver, CO
CNO Code OP 23, Washington, DC
COMSUBDEVGRUONE Ops Offr, San Diego, CA
DTIC Alexandria, VA
DTNSRDC Code 172, Bethesda, MD; DET, Code 522 (Library), Annapolis, MD
EPA ANR-458, Washington, DC
LIBRARY OF CONGRESS Sci & Tech Div, Washington, DC
MARITIME ADMIN B&D, Washington, DC
MCRD SCE, San Diego CA
NAVCOASTSYSCEN Code 2360, Panama City, FL; Tech Library, Panama City, FL
NAVFACENGCOM Code 03, Alexandria, VA; Code 0320 (R. Peloquin), Alexandria, VA; Code 04B (M. Yachnis), Alexandria, VA; Code FPO-3A2 (Bloom), Alexandria, VA; Code FPO-3C, Alexandria, VA
NAVFACENGCOM - CHES DIV, Code FPO-1PL, Washington, DC
NAVFACENGCOM - LANT DIV, Library, Norfolk, VA
NAVFACENGCOM - NORTH DIV, Code 04AL, Philadelphia, PA
NAVFACENGCOM - PAC DIV, Code 402, RDT&E LnO, Pearl Harbor, HI; Library, Pearl Harbor, HI
NAVFACENGCOM - SOUTH DIV, Library, Charleston, SC
NAVFACENGCOM - WEST DIV, Library (Code 04A2.2), San Bruno, CA
NAVOCEANO Library Bay St. Louis, MS
NAVOCEANSYSCEN Code 5204 (J. Stachiw), San Diego, CA
NAVPGSCOL Haderlie, Monterey, CA
NAVSEASYSCOM Code 644, Washington, DC; SEA-05R4 (J. Freund), Washington, DC; Code SEA-99611, Washington, DC
NAVWARCOL Lib Serials, Newport, RI
NOAA M Ringenbach, Rockville, MD; Joseph Vadus, Rockville, MD
NRL Code 5800, Washington, DC
ONR Code 1121 (EA Silva), Arlington, VA
PWC Code 101 (Library), Oakland, CA; Code 123-C, San Diego, CA; Code 420, Great Lakes, IL; Library, Guam, Mariana Islands; Library, Norfolk, VA; Library (Code 134), Pearl Harbor, HI; Library, Pensacola, FL; Tech Library, Subic Bay, RP; Library, Yokosuka JA
SUBRESCUE Sea Cliff DSV4, OIC, San Diego, CA; Turtle DSV-3, OIC, San Diego, CA
HAYNES & ASSOC H. Haynes, P.E., Oakland, CA
U.S. MERCHANT MARINE ACADEMY Reprint Custodian, Kings Point, NY
US GEOLOGICAL SURVEY E Dyhrkopp, Metairie, LA; Marine Oil & Gas Ops (R Krahl), Reston, VA
WATER & POWER RESOURCES SERVICE Smoak, Denver, CO
BROOKHAVEN NATL LAB M. Steinberg, Upton, NY
CALIFORNIA STATE UNIVERSITY Energy Tech Dept (Kohan), Menlo Park, CA; CE Dept (YC Kim), Los Angeles, CA
CLARKSON COLL OF TECH CE Dept (Batson), Potsdam, NY
UNIVERSITY OF CALIFORNIA Prof L.G. Selena, Los Angeles, CA
DAMES & MOORE LIBRARY Los Angeles, CA
DUKE UNIV MEDICAL CENTER CE Dept (Muga), Durham, NC
FLORIDA ATLANTIC UNIVERSITY Ocean Engrg Dept (Hartt), Boca Raton, FL
FLORIDA INSTITUTE OF TECHNOLOGY J Schwalbe, Melbourne, FL
GEORGIA INSTITUTE OF TECHNOLOGY CE Scol (Kahn), Atlanta, GA
INSTITUTE OF MARINE SCIENCES Dir, Port Aransas, TX
JOHNS HOPKINS UNIV Ches Bay Rsch Inst, Rsch Lib, Shady Side, MD
LEHIGH UNIVERSITY CE Dept, Hydraulics Lab, Bethlehem, PA
MIT Lib, Tech Reports, Cambridge, MA
NATURAL ENERGY LAB Library, Honolulu, HI
OKLAHOMA STATE UNIV CE Scol (Lloyd), Stillwater, OK
SEATTLE UNIVERSITY CE Dept (Schwaegler), Seattle, WA
SOUTHWEST RSCH INST R. DeHart, San Antonio TX
STATE UNIVERSITY OF NEW YORK Mat Sci Dept (Herman), Stony Brook, NY
TEXAS A&M UNIVERSITY Hyd Rsch Lab, College Station, TX; CE Dept (Niedzwecki), College Station, TX; CE Dept (Ledbetter), College Station, TX
UNIVERSITY OF CALIFORNIA CE Dept (Gerwick), Berkeley, CA; CE Dept (Pintz), Berkeley, CA; Naval Arch Dept, Berkeley, CA; CE Dept (Polivka), Berkeley, CA; Engrg Lib, Berkeley, CA; CE Dept (Mehta), Berkeley, CA
UNIVERSITY OF DELAWARE CE Dept, Ocean Engrg (Dalrymple), Newark, DE

UNIVERSITY OF ILLINOIS CE Dept (Hall), Urbana, IL; Metz Ref Rm, Urbana, IL; CE Dept (W. Gamble), Urbana, IL
UNIVERSITY OF MASSACHUSETTS ME Dept (Heroneumus), Amherst, MA
UNIVERSITY OF MICHIGAN CE Dept (Berg), Ann Arbor, MI; CE Dept (Richart), Ann Arbor, MI
UNIVERSITY OF NOTRE DAME CE Dept (Katona), Norte Dame, IN
UNIVERSITY OF TEXAS AT AUSTIN Breen, Austin, TX
UNIVERSITY OF TEXAS MEDICAL BRANCH Structural Engrg (Dr. R.L. Yuan), Arlington, TX
UNIVERSITY OF WASHINGTON CE Dept (N. Hawkins), Seattle, WA; CE Dept (Mattock), Seattle, WA; Library, Seattle, WA
WOODS HOLE OCEANOGRAPHIC INST. Doc Lib, Woods Hole, MA
AGBABIAN ASSOC C. Bagge, El Segundo CA
ALFRED A YEE & ASSOC Librarian, Honolulu, HI
AMETEK OFFSHORE RSCH Santa Barbara, CA
ARVID GRANT & ASSOC Olympia, WA
BECHTEL CORP R. Leonard, San Francisco CA
BROWN & ROOT Ward, Houston, TX
CANADA Ontario Hydro (Burnett), Toronto; University of New Brunswick (T.W. Bremnar), Fredericton
CHEVRON OIL FLD RSCH CO Brooks, La Habra, CA
CONCRETE TECH CORP A. Anderson, Tacoma, WA
CONSTRUCTION TECH LABS AE Fiorato, Skokie, IL
CONTINENTAL OIL CO O. Maxson, Ponca City, OK
DILLINGHAM PRECAST F McHale, Honolulu, HI
DIXIE DIVING CENTER Decatur, GA
LIN OFFSHORE ENGRG P. Chow, San Francisco CA
MOBIL R & D CORP Mgr, Offshore Engr, Dallas, TX
NORWAY Inst of Bldg Matrls, Prof O.E. Gjorv, Trondheim
PORTLAND CEMENT ASSOC E Hognestad, Skokie, IL; Corley, Skokie, IL; Rsch & Dev Lab Lib, Skokie, IL
SANDIA LABORATORIES Seabed Prgms (Anderson), Albuquerque, NM
SCHUPACK SUAREZ ENGRS, INC M. Schupack, Norwalk, CT
SHELL OIL CO E&P Civil Engrg, Houston, TX; Boaz, Houston, TX
UNITED KINGDOM OFFSHORE ENGINEER (A. Cottrill, Ed), London
DOBROWOLSKI, JA Altadena, CA